PLOS GENETICS

RESEARCH ARTICLE

Reduced coenzyme Q synthesis confers non-target site resistance to the herbicide thaxtomin A

Chloe Casey[1,2], Thomas Köcher[3], Clément Champion[1], Katharina Jandrasits[2], Magdalena Mosiolek[2], Clémence Bonnot[1], Liam Dolan[1,2]*

1 Department of Biology, University of Oxford, Oxford, United Kingdom, **2** Gregor Mendel Institute, Vienna, Austria, **3** Vienna Biocenter Core Facilities, Vienna, Austria

* liam.dolan@gmi.oeaw.ac.at

Citation: Casey C, Köcher T, Champion C, Jandrasits K, Mosiolek M, Bonnot C, et al. (2023) Reduced coenzyme Q synthesis confers non-target site resistance to the herbicide thaxtomin A. PLoS Genet 19(1): e1010423. https://doi.org/10.1371/journal.pgen.1010423

Editor: Claudia Köhler, Max Planck Institute of Molecular Plant Physiology: Max-Planck-Institut fur molekulare Pflanzenphysiologie, GERMANY

Received: September 16, 2022

Accepted: December 21, 2022

Published: January 6, 2023

Data Availability Statement: All relevant data are within the paper and its Supporting Information files.

Funding: This research was supported by a European Research Council (ERC) (https://erc.europa.eu/) Advanced Grants EVO500 (project number 250284) and De Novo-P (project number 787613) to L.D. from the European Commission. Ch. Ca. was supported by the Biotechnology and Biological Sciences Research Council (BBSRC)

Abstract

Herbicide resistance in weeds is a growing threat to global crop production. Non-target site resistance is problematic because a single resistance allele can confer tolerance to many herbicides (cross resistance), and it is often a polygenic trait so it can be difficult to identify the molecular mechanisms involved. Most characterized molecular mechanisms of non-target site resistance are caused by gain-of-function mutations in genes from a few key gene families–the mechanisms of resistance caused by loss-of-function mutations remain unclear. In this study, we first show that the mechanism of non-target site resistance to the herbicide thaxtomin A conferred by loss-of-function of the gene *PAM16* is conserved in *Marchantia polymorpha*, validating its use as a model species with which to study non-target site resistance. To identify mechanisms of non-target site resistance caused by loss-of-function mutations, we generated 10^7 UV-B mutagenized *M. polymorpha* spores and screened for resistance to the herbicide thaxtomin A. We isolated 13 thaxtomin A-resistant mutants and found that 3 mutants carried candidate resistance-conferring SNPs in the Mp*RTN4IP1L* gene. Mp*rtn4ip1l* mutants are defective in coenzyme Q biosynthesis and accumulate higher levels of reactive oxygen species (ROS) than wild-type plants. Mutants are weakly resistant to thaxtomin A and cross resistant to isoxaben, suggesting that loss of Mp*RTN4IP1L* function confers non-target site resistance. Mutants are also defective in thaxtomin A metabolism. We conclude that loss of Mp*RTN4IP1L* function is a novel mechanism of non-target site herbicide resistance and propose that other mutations that increase ROS levels or decrease thaxtomin A metabolism could contribute to thaxtomin A resistance in the field.

Author summary

Intensive agriculture relies on herbicides to control weed populations. However, herbicide resistance in weeds threatens the efficacy of herbicides and global crop production, similar to how antibiotic resistance poses a global health threat. Understanding the molecular mechanisms behind herbicide resistance helps to prevent resistance from evolving and to better manage herbicide resistant weeds in the field. Here, we use a forward genetic

(https://www.ukri.org/councils/bbsrc/) Scholarship through a doctoral training programme (grant number BB/M011224/1). Cl. Ch. was supported by a Clarendon Scholarship of Oxford University and the Sidney Perry foundation (https://www.the-sidney-perry-foundation.co.uk/). C.B. was funded by the PLANTORIGINS network (project number 238640) to L.D. from the European Commission. The funders had no role in study design, data collection and analysis, decision to publish, or preparation of the manuscript.

Competing interests: I have read the journal's policy and the authors of this manuscript have the following competing interests: L.D. and Cl. Ch. are co-founders of MoA Technology Ltd.

approach in the model species *Marchantia polymorpha* to discover novel mechanisms of herbicide resistance. We report the discovery of a novel mechanism of herbicide resistance caused by loss-of-function mutations in the Mp*RTN4IP1L* gene. We find that Mp*rtn4ip1l* mutants are resistant to the herbicides thaxtomin A and isoxaben, accumulate higher levels of reactive oxygen species than wild type plants, and are defective in thaxtomin A metabolism. We predict that loss-of-function mutations or treatments that increase reactive oxygen species production could contribute to thaxtomin A resistance.

Introduction

The control of weeds by herbicides is threatened by the evolution of resistance in the field [1,2]. This is analogous to how human and animal health is threatened by the evolution of antibiotic resistance in bacteria. The intense selection pressure resulting from herbicide treatments can lead to the rapid evolution of herbicide resistance in the agricultural landscape [1]. Resistance can result from genetic changes in the gene encoding the herbicide target which lead to conformational changes in the target protein blocking herbicide binding, or overexpression of the target [3,4]. This form of resistance, which involves mutations only in the gene encoding the target protein, is known as target-site resistance. Plants with a target-site resistance mutation can be very strongly resistant to herbicides [1]. For example, target-site resistant biotypes of the weed *Euphorbia heterophylla* survive more than 50 times the recommended field dose of the acetohydroxyacid synthase (AHAS) inhibitor imazamox [5]. Resistance can also result from genetic changes in a variety of genes which prevent inhibitory levels of herbicide reaching the target, or that alleviate the toxic effects of the herbicide downstream from the target [1,3,6]. For example, a mutation which causes constitutive expression of a glutathione transferase gene confers resistance in the weed species *Alopecurus myosuroides*. In this example, resistance is the result of increased herbicide metabolism and increased accumulation of flavonol metabolites that act as antioxidants. Accumulation of these molecules can confer resistance to herbicides whose toxicity depends on the accumulation of toxic reactive oxygen species [7–9]. These types of resistance–which do not involve mutations in the gene encoding the herbicide target–are known as non-target site resistance. Individual alleles that contribute to non-target site resistance usually confer weaker resistance to herbicides than alleles responsible for target-site resistance [10].

Both target-site and non-target site resistance can be caused by gain-of-function mutations, which cause an increase in expression of a gene or enhanced activity of a protein. For example, the 5-enolpyruvyl shikiminate-3-phosphate synthase (EPSPS) gene encodes a protein essential for aromatic amino acid biosynthesis which is the target of the herbicide glyphosate [11]. Gain-of-function mutations in the gene encoding EPSPS resulting in gene amplification (multiple rounds of gene duplication) confer target-site resistance to the herbicide glyphosate [12,13]. EPSPS gene copy number is greater in many glyphosate-resistant populations than in glyphosate-sensitive populations, resulting in higher steady state levels of EPSPS mRNA, protein, and total enzyme activity. The resulting elevated levels of EPSPS activity increase glyphosate resistance [13]. Non-target site resistance can also be conferred by spontaneous gain-of-function mutations in genes encoding enzyme activities that chemically modify or compartmentalize herbicides and prevent the herbicide reaching the target [1,6,14]. For example, constitutive overexpression of an ABC transporter causing glyphosate export into the apoplast results in glyphosate resistance in *E. colona* [15].

Loss-of-function mutations–mutations that result in reduced gene and protein function–can also cause target-site resistance. This is because mutations in the gene encoding a herbicide target which cause conformational changes that prevent herbicide binding can also reduce the capacity of the protein to carry out its function. For example, some mutations in EPSPS that confer glyphosate resistance by preventing the binding of glyphosate also reduce the affinity of EPSPS for its substrate phosphoenolpyruvate, leading to reduced catalytic activity [16]. However, very few loss-of-function mutations causing non-target site resistance have been reported in weeds. Recent genome wide association studies have identified mutations associated with glyphosate resistance in the weed species *Amaranthus tuberculatus* and *Ipomoea purpurea* of which some are likely to be loss-of-function, suggesting that the contribution of loss-of-function mutations to non-target site resistance has been underestimated, however the contribution of these mutations to resistance has not yet been experimentally confirmed [17–19]. Only two mechanisms of non-target site resistance involving loss-of-function mutations have been proven to confer resistance, using forward genetics in the model species *Arabidopsis thaliana* [20,21]. As such, the role of loss-of-function mutations in non-target site resistance in weeds is unclear.

It is likely that both gain- and loss-of-function mutations contribute to non-target site resistance in herbicide resistant weed populations, but it is difficult to identify resistance mechanisms of non-target site resistance, including those conferred by loss of gene function. This is partly because non-target site resistance is usually a polygenic trait, and each single allele may contribute little to resistance. For example, in a sample of glyphosate resistant *A*. *tuberculatus* individuals, it was estimated that 25% of the variance in resistance was attributed to non-target site resistance associated with SNPs in 274 genes with a range of allele frequencies and effect sizes [17,19]. Identifying the mutant genes that contribute such a small amount to total resistance phenotypes is challenging in weeds. This makes defining the molecular basis of non-target site resistance difficult. The few alleles which have been identified are those which have a large effect on resistance. So far, these have all been gain-of-function alleles involving genes from a few key gene families such as cytochrome P450s, glutathione-S-transferases, glycosyltransferases, and ABC transporters [6]. There are likely a variety of undiscovered non-target site resistance causing mutations which each have a small effect on resistance but additively cause strong resistance. Identifying these diverse mechanisms of non-target site resistance–which likely include loss-of-function mutations–remains a challenge.

We set out to identify mechanisms of non-target site resistance to thaxtomin A–a natural product being developed as a herbicide–caused by loss-of-function mutations. We chose thaxtomin A because it has been approved by the US Environmental Protection Agency as a herbicide (EPA registration number 84059–12) [22–28]. Thaxtomin A is thought to act by inhibiting plant cell wall biosynthesis, a process necessary for plant growth and the inhibition of which leads to plant death [29, 30]. This plant specific mode of action makes thaxtomin A a favourable herbicide choice due to its low toxicity to animals. To date, only one mechanism of resistance to thaxtomin A has been identified (via forward mutagenesis in *Arabidopsis thaliana*) caused by loss-of-function mutations in *PAM16*, which encodes a member of the TIM complex, involved in protein transport into mitochondria [20,31,32].

To identify novel loss-of-function mutations that confer resistance to thaxtomin A, we UV mutagenized a large population of *Marchantia polymorpha* spores and screened for mutants which survived the lethal dose of thaxtomin A. We chose *M*. *polymorpha* as a model species because a single female sporophyte produces millions of haploid spores which can be mutagenized and directly screened for resistance. This enables rapid mutant screens in large populations that would be difficult to carry out at the same scale in diploid flowering plant models [33,34]. Furthermore, there is evidence that gene networks underlying bryophyte gametophyte

physiology and development are similar to those in angiosperms [35, 36]. We identified 13 thaxtomin A-resistant mutants. Three independent mutants carried candidate resistance-conferring mutations in the Mp*RTN4IP1L* gene, which functions in the biosynthesis of coenzyme Q, a component of the mitochondrial electron transport chain. Mp*rtn4ip1l* mutants accumulated higher levels of reactive oxygen species (ROS) than wild type controls and were defective in thaxtomin A metabolism. Taken together these data suggest that mutations that lead to ROS accumulation or which hinder thaxtomin A metabolism may confer resistance to thaxtomin A. We predict that loss-of-function mutations that increase ROS levels or decrease thaxtomin A metabolism in weeds will confer resistance to thaxtomin A in the field.

Results

A mechanism of non-target site resistance conferred by loss-of-function of *PAM16* is conserved in *M. polymorpha*

To determine if *M. polymorpha* is a suitable model species for discovering novel mechanisms of non-target site resistance to thaxtomin A, we first tested if *M. polymorpha* is sensitive to thaxtomin A. Wild type gemmae from Takaragaike-1 (Tak-1) and Takaragaike-2 (Tak-2) accessions were grown on solid medium supplemented with different concentrations of thaxtomin A. The area of living tissue of these plants was measured after 14 days (Fig 1A and Tab A in S1 Table). Thaxtomin A treatment inhibits the growth of wild type *M. polymorpha* in a dose-dependent manner (Fig 1A and 1B). The IC_{50} (dose at which average area of living tissue is reduced by 50%) was 56 ± 6 nM for Tak-1, and 135 ± 24 nM for Tak-2. The LD_{100} (lethal dose at which no plant tissue is alive) for both Tak-1 and Tak-2 was 5 μM, although in rare cases Tak-1 can survive this dose (Fig 1A and 1B).

To validate the suitability of *M. polymorpha* to study non-target site resistance to thaxtomin A, we tested whether a known mechanism of non-target site thaxtomin A resistance discovered in *Arabidopsis thaliana* is conserved in *M. polymorpha*. Loss-of-function mutations in the At*PAM16* gene (AT3G59280) confer non-target site resistance to thaxtomin A in *A. thaliana* [20, 32]. *PAM16* encodes a subunit of the PAM/TIM complex that transports proteins across the inner mitochondrial membrane [31]. We tested the hypothesis that loss of *PAM16* function confers thaxtomin A resistance in *M. polymorpha*.

The closest homologue of At*PAM16* in *M. polymorpha* was identified by BlastP as Mp3g09390.1 [37]. To determine the evolutionary history of the *PAM16* gene and determine if Mp3g09390.1 is the only copy of PAM16 in *M. polymorpha*, a phylogeny was created of the homologues of *PAM16* from 11 different species (Figs 1C and S1A and S1B and S2 Table and S1 Text). There were between one and three copies of *PAM16* in each species and there was one copy in *M. polymorpha* (Mp3g09390.1). Mp3g09390.1 is therefore the only *PAM16* gene in the *M. polymorpha* genome and will be referred to as Mp*PAM16*.

To determine if loss of Mp*PAM16* function confers thaxtomin A resistance, Mp*pam16* loss-of-function mutants were generated using CRISPR-Cas9 mutagenesis. Guide RNAs were designed to generate mutations in the highly conserved N-terminal predicted signal peptide which targets the PAM16 protein to the inner mitochondrial membrane (sgRNA 2), and a non-conserved region at the C-terminal end of the protein (sgRNA 1) (Fig 1D). Thirty-three Mp*pam16* mutants were generated. The highly conserved signal peptide was mutated in 28 Mp*pam16* mutants; the non-conserved C-terminal region of the protein was mutated in the 5 remaining Mp*pam16* mutants.

Gemmae from the Mp*pam16* mutant lines were grown on solid medium supplemented with 5 μM thaxtomin A (LD_{100}) (Fig 1E) or 0.1% DMSO (Fig 1F). The area of living plant tissue was quantified after 12 days of growth (Tabs B and C in S1 Table). Mp*pam16* mutant lines

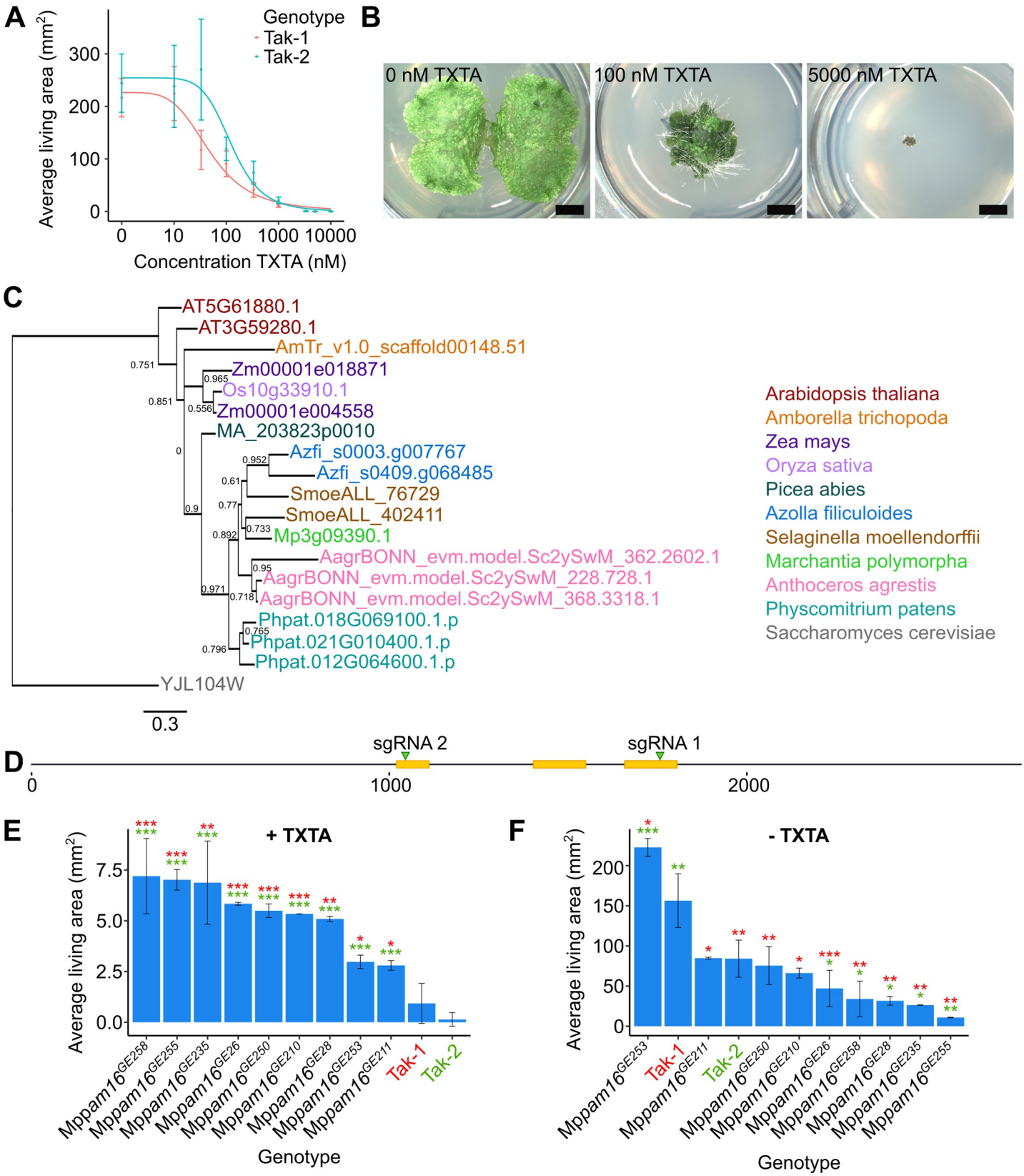
A
Average living area (mm²)
Genotype
Tak-1
Tak-2
Concentration TXTA (nM)
B
0 nM TXTA
100 nM TXTA
5000 nM TXTA
C
AT5G61880.1
AT3G59280.1
AmTr_v1.0_scaffold00148.51
Zm00001e018871
Os10g33910.1
Zm00001e004558
MA_203823p0010
Azfi_s0003.g007767
Azfi_s0409.g068485
SmoeALL_76729
SmoeALL_402411
Mp3g09390.1
AagrBONN_evm.model.Sc2ySwM_362.2602.1
AagrBONN_evm.model.Sc2ySwM_228.728.1
AagrBONN_evm.model.Sc2ySwM_368.3318.1
Phpat.018G069100.1.p
Phpat.021G010400.1.p
Phpat.012G064600.1.p
YJL104W
0.3
Arabidopsis thaliana
Amborella trichopoda
Zea mays
Oryza sativa
Picea abies
Azolla filiculoides
Selaginella moellendorffii
Marchantia polymorpha
Anthoceros agrestis
Physcomitrium patens
Saccharomyces cerevisiae
D
sgRNA 2
sgRNA 1
E
+ TXTA
Average living area (mm²)
Genotype
F
- TXTA
Average living area (mm²)
Genotype

Fig 1. A mechanism of non-target site resistance conferred by loss-of-function of *PAM16* is conserved in *M. polymorpha*. **A:** Dose-response curves of the growth of wild type lines on thaxtomin A (TXTA). Wild type gemmae (Tak-1 and Tak-2) were grown for 14 days on solid medium supplemented with different concentrations of thaxtomin A (Tab A in S1 Table). The fitted curves and IC_{50} values were calculated using the four-parameter log-logistic equation. Error bars represent ± standard deviation (n = 18). **B:** Wild type (Tak-1) gemmalings grown for 12 days on solid medium supplemented with DMSO, 100 nM thaxtomin A, or 5000 nM thaxtomin A. Images were taken with a Keyence VHX-7000. Scale bars represent 2 mm and were added in Inkscape v1.0.1. **C:** Phylogenetic analysis of *PAM16* in plants. Proteins similar to AtPAM16 (At3G59280) were identified by protein BLAST search (E value < 1E-5) against the reference proteomes of various species (S2 Table and S1 Text) [37]. Orthologues were aligned and a maximum likelihood analysis was conducted. The tree was rooted with the *PAM16* homologue from *S. cerevisiae*. A non-parametric approximate likelihood ratio test based on a Shimodaira-Hasegawa-like procedure was used to calculate branch support values [38]. **D:** Schematic representation of the Mp*PAM16* (Mp3g09390.1) gene constructed using Inkscape v1.0.1. CDS regions are represented in yellow. The regions of the gene targeted by guide RNAs are marked with green arrowheads. **E and F:** Wild type gemmae (Tak-1 and Tak-2) and gemmae from the nine thaxtomin A-resistant Mp*pam16* mutants were grown for 12 days on solid medium supplemented with 5 μM thaxtomin A (**E**) (Tab B in S1 Table) or 0.1% DMSO (**F**) (Tab C in S1 Table). The fitted curves and IC_{50} values were calculated using the four-parameter log-logistic equation. Error bars represent ± standard deviation (n = 2–7). Stars represent the level of significance (as determined by Student's t-tests) of the difference between mutant and control lines (comparison to Tak-1 in red and Tak-2 in green): * = $p < 0.05$, ** = $p < 0.01$, *** = $p < 0.001$.

https://doi.org/10.1371/journal.pgen.1010423.g001

which were significantly larger than wild type plants on thaxtomin A were classed as resistant. Nine Mp*pam16* lines were significantly larger than both Tak-1 and Tak-2 on 5 μM thaxtomin A and therefore classed as thaxtomin A-resistant ($p < 0.05$) (Fig 1E).

Five of the nine thaxtomin A-resistant Mp*pam16* mutants were significantly smaller than Tak-1 and Tak-2 plants in control conditions, including the four Mp*pam16* mutants which grew largest on thaxtomin A–Mp$pam16^{GE258}$, Mp$pam16^{GE255}$, Mp$pam16^{GE235}$, and Mp$pam16^{GE26}$ (Fig 1F). This suggests that growth defects are more likely in Mp*pam16* mutant lines with stronger resistance to thaxtomin A.

All 9 thaxtomin A-resistant Mp*pam16* mutants were mutated in the highly conserved region that comprises the predicted PAM16 signal peptide (S1C Fig). The mutations in the thaxtomin A-resistant mutants affect between 2 and 19 amino acids and involve a range of substitutions, insertions, and deletions (S1C Fig). A mutation in the signal peptide is predicted to disrupt PAM16 function by preventing its transport to the mitochondria. These mutations are therefore likely to be loss-of-function. Given that all 9 thaxtomin A-resistant Mp*pam16* mutant lines carry likely loss-of-function mutations, we conclude that loss-of-function of Mp*pam16* can confer thaxtomin A resistance. The resistance of Mp*pam16* mutants to thaxtomin A validates *M. polymorpha* as a model to identify novel mechanisms of non-target site resistance to this herbicide.

13 thaxtomin A-resistant *M. polymorpha* mutants were isolated from a screen of 10^7 mutants

A genetic screen was carried out to identify mutants resistant to the herbicide thaxtomin A. To generate thaxtomin A-resistant mutants, 2 x 10^7 wild type *M. polymorpha* spores were plated on solid medium supplemented with 5 μM thaxtomin A and exposed to UV-B irradiation to induce mutations. A screening dose of 5 μM thaxtomin A (LD_{100}) was selected as screening at the lethal dose (as opposed to higher than the lethal dose) preferentially selects for non-target site resistance [39]. The dose of UV-B radiation used killed approximately 50% of spores (S2 Fig and Tab D in S1 Table). Ten million mutagenized spores were screened for resistance to thaxtomin A 14 days after mutagenesis (Fig 2A). Resistant mutants were transferred to fresh solid medium supplemented with 5 μM thaxtomin A to confirm their resistance. Mutants that survived the second round of selection were retained, and gemmae from each resistant mutant were plated onto fresh solid medium supplemented with 5 μM thaxtomin A to verify the retention of resistance through asexual reproduction (Fig 2B). Mutant gemmae that survived and grew significantly larger than wild type gemmae on 5 μM thaxtomin A were classed as thaxtomin A-resistant (Fig 2C and Tab E in S1 Table). Using this protocol, 13 thaxtomin A-resistant

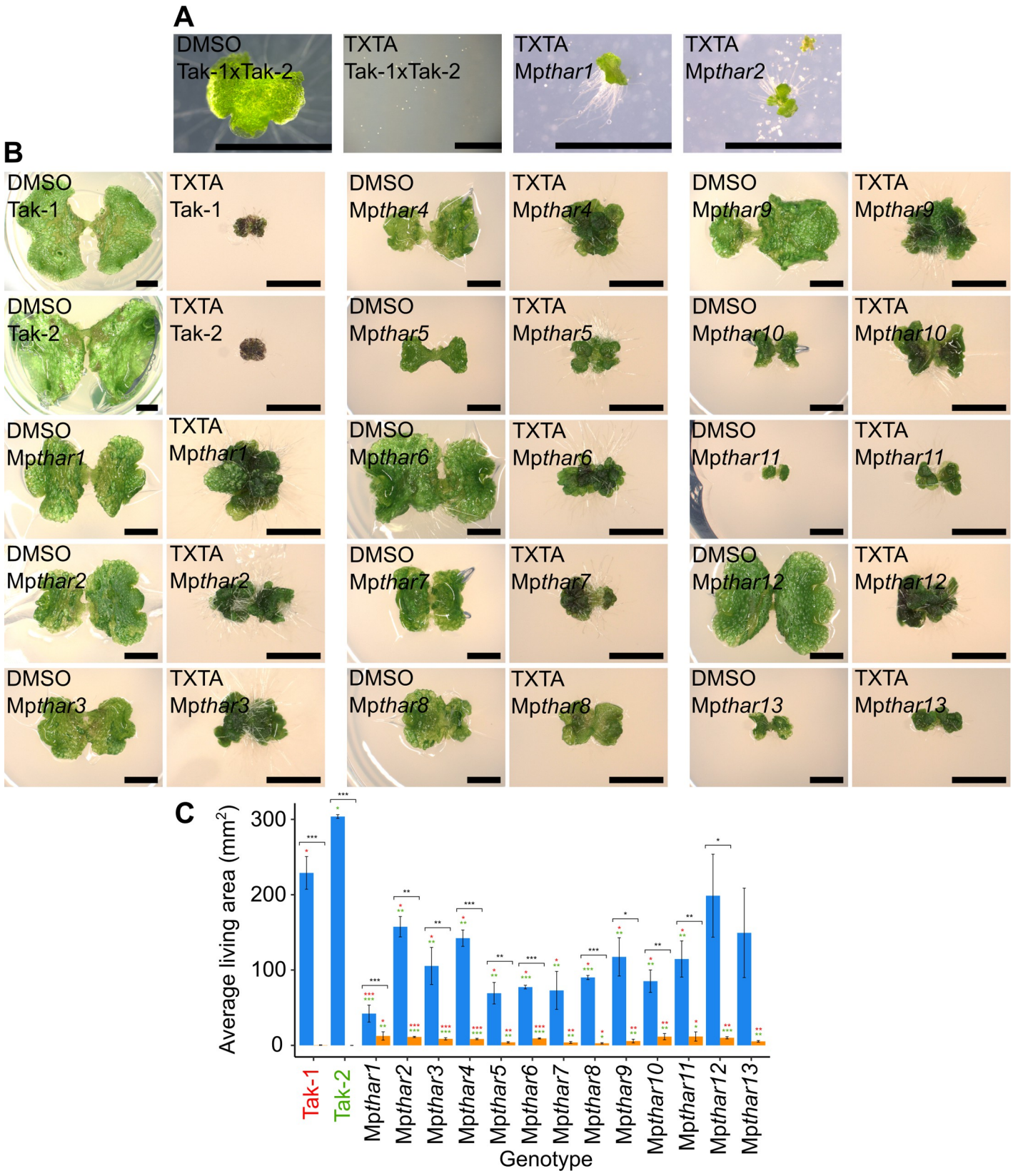
A
DMSO
Tak-1xTak-2
TXTA
Tak-1xTak-2
TXTA
Mpthar1
TXTA
Mpthar2
B
DMSO
Tak-1
TXTA
Tak-1
DMSO
Mpthar4
TXTA
Mpthar4
DMSO
Mpthar9
TXTA
Mpthar9
DMSO
Tak-2
TXTA
Tak-2
DMSO
Mpthar5
TXTA
Mpthar5
DMSO
Mpthar10
TXTA
Mpthar10
DMSO
Mpthar1
TXTA
Mpthar1
DMSO
Mpthar6
TXTA
Mpthar6
DMSO
Mpthar11
TXTA
Mpthar11
DMSO
Mpthar2
TXTA
Mpthar2
DMSO
Mpthar7
TXTA
Mpthar7
DMSO
Mpthar12
TXTA
Mpthar12
DMSO
Mpthar3
TXTA
Mpthar3
DMSO
Mpthar8
TXTA
Mpthar8
DMSO
Mpthar13
TXTA
Mpthar13
C
Average living area (mm²)
300
200
100
0
Tak-1
Tak-2
Mpthar1
Mpthar2
Mpthar3
Mpthar4
Mpthar5
Mpthar6
Mpthar7
Mpthar8
Mpthar9
Mpthar10
Mpthar11
Mpthar12
Mpthar13
Genotype

Fig 2. 13 thaxtomin A-resistant mutants were isolated from a screen of 10^7 mutants. A: Wild type spores from a cross between Tak-1 and Tak-2 grown for 14 days on solid medium supplemented with 0.1% DMSO or 5 μM thaxtomin A (TXTA), and UV-B mutagenesis selection plates supplemented with 5 μM thaxtomin A showing 14-day old thaxtomin A-resistant mutants Mp*thar*1 and Mp*thar*2 surrounded by dead mutagenized thaxtomin A-sensitive spores. Images were taken with a Leica DFC310 FX stereomicroscope. Scale bars represent 2 mm and were added in Inkscape v1.0.1. **B:** Wild type (Tak-1 and Tak-2) and Mp*thar* gemmalings grown for 12 days on solid medium supplemented with 0.1% DMSO or 5 μM thaxtomin A. Images were taken with a Keyence VHX-7000 and the maximum pixel value was adjusted to 188 in ImageJ. Scale bars represent 2 mm and were added in Inkscape v1.0.1. **C:** Gemmae from wild type lines (Tak-1 and Tak-2) and from Mp*thar* lines were plated on solid medium supplemented with DMSO (blue bars) or 5 μM thaxtomin A (orange bars) and grown for 21 days (n = 3–13) (Tab E in S1 Table). Error bars represent ± standard deviation. Stars represent the level of significance (as determined by Student's t-tests) of the difference between mutant and control lines subjected to the same treatment (comparison to Tak-1 in red and Tak-2 in green), or between individuals of the same genotype subjected to different treatments (black): * = $p < 0.05$, ** = $p < 0.01$, *** = $p < 0.001$.

https://doi.org/10.1371/journal.pgen.1010423.g002

Mp*thar* (*th*axtomin *A r*esistant) mutant lines were identified out of the 10^7 mutagenized spores screened.

The Mp*RTN4IP1L* gene is mutated in three Mp*thar* mutants

To identify mutations that confer thaxtomin A resistance, the genome of each Mp*thar* mutant was sequenced and the most likely resistance-conferring SNP in each mutant was identified using a modified version of a SNP calling bioinformatic pipeline adapted from [40]. Mismatches in the genomes of Mp*thar* mutants were compared to mismatches in the genomes of thaxtomin A-sensitive plants (Tak-1, Tak-2, and thaxtomin A-sensitive UV-B mutants [40]). Mismatches found only in Mp*thar* mutants and which passed further filtering steps were considered to be candidate resistance-conferring mutations. Between 6 and 27 candidate resistance-conferring mutations were identified for each Mp*thar* mutant. These SNPs were compared between Mp*thar* mutants. There were candidate resistance-conferring SNPs in the Mp3g19030.1 gene in 3 independent Mp*thar* mutants (Mp*thar2*, Mp*thar4*, and Mp*thar6*) (Fig 3A and 3B). The presence of these SNPs was confirmed by Sanger sequencing (S3A, S3B and S3C Fig). Given that the Mp3g19030.1 gene carries a candidate resistance-conferring mutation in 3 independent Mp*thar* mutants, it is likely that a mutation in Mp3g19030.1 confers thaxtomin A resistance.

Mp3g19030.1 is annotated in the reference *M. polymorpha* genome (MpTak v6.1) as a homologue of the *H. sapiens RETICULON 4-INTERACTING PROTEIN 1.1* (Hs*RTN4IP1.1*) gene. Hs*RTN4IP1.1* encodes a mitochondrial NADH oxidoreductase involved in the biosynthesis of coenzyme Q, and its homologue *RAD-8* was first discovered in *C. elegans* [41,42]. To determine the phylogenetic relationship between Mp3g19030.1 and its homologues, gene trees were generated from the homologs of Hs*RTN4IP1* from 10 species (Figs 3C and S3D and Table 1 and S1 Text). There were between 4 and 8 Hs*RTN4IP1.1* homologues in each of the species analyzed (Table 1). The homologues group into a clade of 2-methylene-furan-3-one reductases (support value 1), a clade containing Hs*RTN4IP1.1* and its closest homologues (support value 0.9151), and a clade containing quinone oxidoreductases, alcohol dehydrogenases, and prostaglandin reductases (support value 0.8706) (Fig 3C). Based on the annotations, the identified homologues of Hs*RTN4IP1.1* therefore likely include enzymes with similar activities.

Mp3g19030.1 forms a clade (support value 0.9997) with Hs*RTN4IP1.1* homologues from *A. thaliana*, *B. distachyon*, and *S. moellendorffii* (AT3G15090.1; E value 6×10^{-54}, BRADI_2g50080v3 isoform 1; E value 2.4×10^{-7}, BRADI_2g50080v3 isoform 2; E value 3.7×10^{-9}, and XP_024530385.1; E value 1×10^{-46}) that is sister to the clade representing the *RAD-8/RTN4IP1* genes from *H. sapiens*, *M. musculus* (*RTN4IP1*; E value 0) and *C. elegans* (*RAD-8*; E value 4×10^{-63}) (support value 0.9691) (Fig 3D).

Mp3g19030.1 is the most closely related *M. polymorpha* homologue of Hs*RTN4IP1.1* gene based on BlastP. However, the topology of the phylogenetic tree suggests that Mp1g20380.1, a

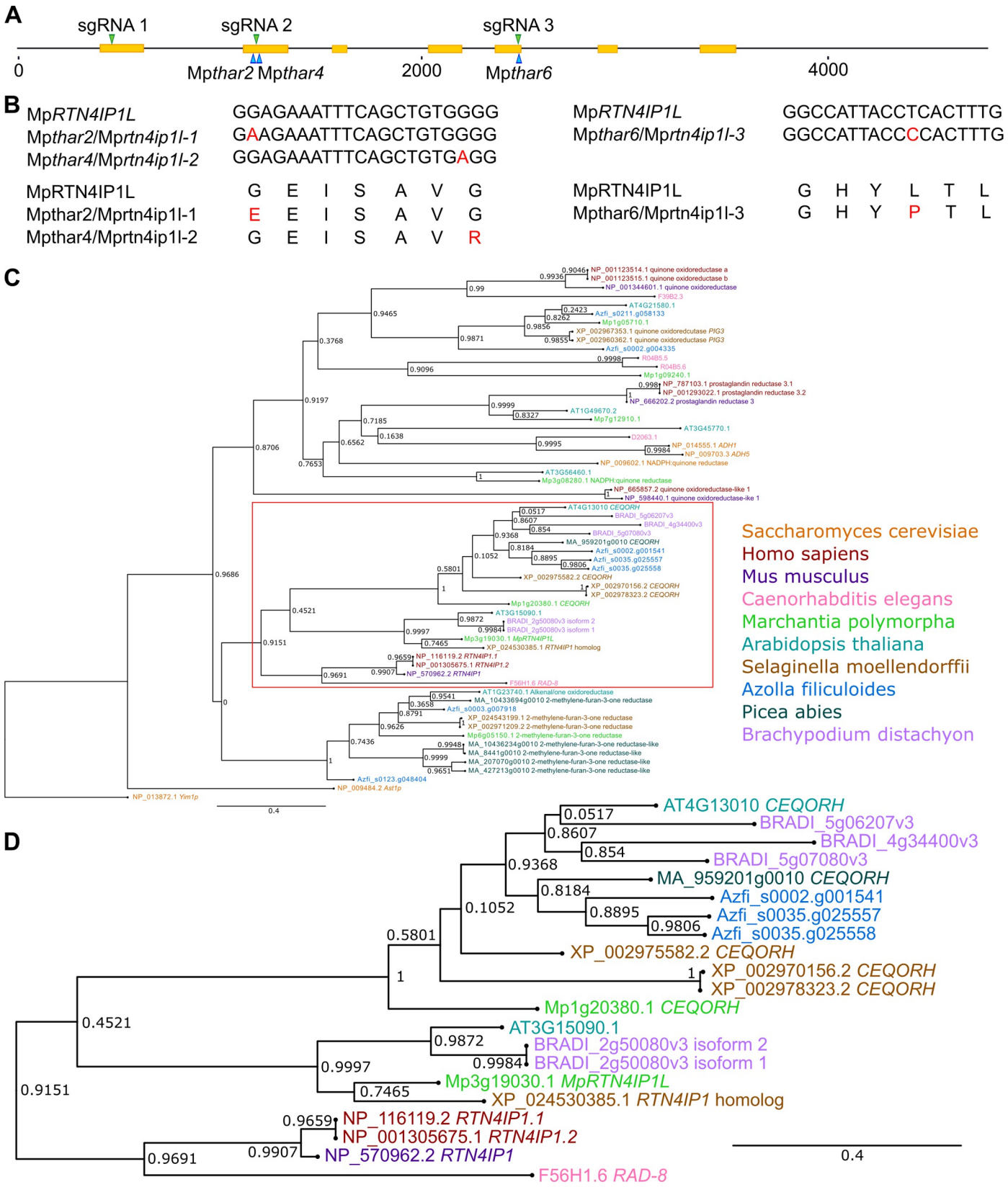
A
sgRNA 1
sgRNA 2
sgRNA 3
0
Mpthar2 Mpthar4
2000
Mpthar6
4000
B
MpRTN4IP1L GGAGAAATTTCAGCTGTGGGG
Mpthar2/Mprtn4ip1l-1 GAAGAAATTTCAGCTGTGGGG
Mpthar4/Mprtn4ip1l-2 GGAGAAATTTCAGCTGTGAGG
MpRTN4IP1L G E I S A V G
Mpthar2/Mprtn4ip1l-1 E E I S A V G
Mpthar4/Mprtn4ip1l-2 G E I S A V R
MpRTN4IP1L GGCCATTACCTCACTTTG
Mpthar6/Mprtn4ip1l-3 GGCCATTACCCCACTTTG
MpRTN4IP1L G H Y L T L
Mpthar6/Mprtn4ip1l-3 G H Y P T L
C
Saccharomyces cerevisiae
Homo sapiens
Mus musculus
Caenorhabditis elegans
Marchantia polymorpha
Arabidopsis thaliana
Selaginella moellendorffii
Azolla filiculoides
Picea abies
Brachypodium distachyon
D
AT4G13010 CEQORH
BRADI_5g06207v3
BRADI_4g34400v3
BRADI_5g07080v3
MA_959201g0010 CEQORH
Azfi_s0002.g001541
Azfi_s0035.g025557
Azfi_s0035.g025558
XP_002975582.2 CEQORH
XP_002970156.2 CEQORH
XP_002978323.2 CEQORH
Mp1g20380.1 CEQORH
AT3G15090.1
BRADI_2g50080v3 isoform 2
BRADI_2g50080v3 isoform 1
Mp3g19030.1 MpRTN4IP1L
XP_024530385.1 RTN4IP1 homolog
NP_116119.2 RTN4IP1.1
NP_001305675.1 RTN4IP1.2
NP_570962.2 RTN4IP1
F56H1.6 RAD-8
0.4

Fig 3. The Mp*RTN4IP1L* (Mp3g19030.1) gene is mutated in 3 Mp*thar* mutants. A: Schematic representation of the Mp*RTN4IP1L* (Mp3g19030.1) gene constructed using Inkscape v1.0.1. CDS regions are represented in yellow. The positions of the SNPs in Mp*thar* are marked with blue arrowheads. The regions of the gene targeted by guide RNAs (sgRNA 1, sgRNA 2, and sgRNA 3) are marked with green arrowheads. **B:** Nucleotide alignments of the wild type Mp*RTN4IP1L* gene and the mutant Mp*rtn41ip1l* genes in Mp*thar* mutants, and amino acid alignments of the MpRTN4IP1L protein and predicted mutant Mprtn4ip1l proteins in Mp*thar* mutants. **C:** Phylogenetic analysis of *RTN4IP1* in eukaryotes. Proteins similar to the human RTN4IP1.1 protein were identified by protein BLAST search (E value < 1E-5) against the reference proteomes of various species (S1 Text) [37]. Orthologues were aligned and a maximum likelihood analysis was conducted. The tree was rooted with the *RTN4IP1* homologue (Yim1p) from *S. cerevisiae*. A non-parametric approximate likelihood ratio test based on a Shimodaira-Hasegawa-like procedure was used to calculate branch support values [38]. **D:** Magnification of the red boxed branch from (**C**) showing that Mp3g19030.1 diverges into a monophyletic clade containing the human *RTN4IP1.1* gene.

https://doi.org/10.1371/journal.pgen.1010423.g003

chloroplast envelope quinone oxidoreductase homologue, is an equally related *M. polymorpha* homologue of Hs*RTN4IP1.1* (Fig 3D). Therefore, Mp3g19030.1 will be referred to as Mp*RTN4IP1-LIKE* (Mp*RTN4IP1L*). At4G13010.1 –the closest *A. thaliana* homolog to Mp1g20380.1 –localizes to the chloroplast envelope [43,44]. At3G15090.1 –the closest *A. thaliana* homologue of Mp*RTN4IP1L* –localizes to the mitochondria in *A. thaliana* leaves [45]. This is consistent with the hypothesis that Mp*RTN4IP1L* is a mitochondrial protein.

Loss-of-function of Mp*RTN4IP1L* is a novel mechanism of herbicide resistance

To independently verify that loss of Mp*RTN4IP1L* function confers thaxtomin A resistance, Mp*rtn4ip1l* loss-of-function mutants were generated using CRISPR-Cas9 targeted mutagenesis. A guide RNA was designed to mutate the beginning of the gene to induce frameshifts (sgRNA 1), and 2 guide RNAs were designed to mutate the sites mutated in Mp*thar*2, Mp*thar*4, and Mp*thar*6 (sgRNA 2 and sgRNA 3) (Fig 3A). In total, 19 Mp*rtn4ip1l* mutants were generated. Based on the nucleotide and predicted protein sequences, there were in frame indels in Mp*rtn4ip1l* which affected 5 or fewer amino acids in the Mprtn4ip1l protein of Mp*rtn4ip1l*^{GE111} and Mp*rtn4ip1l*^{GE117} (S4 Fig). There were large indels or frameshift mutations in Mp*rtn4ip1l* which affected 10 or more amino acids in the Mprtn4ip1l protein of the remaining 17 Mp*rtn4ip1l* mutants, therefore these 17 lines were predicted loss-of-function lines (S4 Fig).

Gemmae from the Mp*rtn4ip1l* mutant lines and from lines with a wild type Mp*RTN4IP1L* (Tak-1, Tak-2, and 3 lines which were transformed with the CRISPR construct but had no mutations in the Mp*RTN4IP1L* gene; Mp*RTN4IP1L*^{GE153}, Mp*RTN4IP1L*^{GE314}, and Mp*RTN4IP1L*^{GE356}) were grown on solid medium supplemented with 5 μM thaxtomin A

Table 1. Species included in the phylogenetic analysis of *RTN4IP1* homologues.

Organism	BLAST tool	Number of *RTN4IP1* homologues (E < 1E-5)
Homo sapiens	NCBI	7
Saccharomyces cerevisiae	NCBI	5
Caenorhabditis elegans	Wormbase	5
Mus musculus	NCBI	4
Marchantia polymorpha	marchantia.info	7
Arabidopsis thaliana	TAIR	7
Selaginella moellendorffii	NCBI	8
Picea abies	Congenie	6
Brachypodium distachyon	Ensembl	5
Azolla filiculoides	Fernbase	7

Proteins similar to HsRTN4IP1.1 were identified via BlastP search of proteomes from these species [37]. Only homologues with an E value < 1 E-5 were included in the analysis.

https://doi.org/10.1371/journal.pgen.1010423.t001

(LD_{100}) (Fig 4A and 4B and Tab F in S1 Table) or 0.1% DMSO (Fig 4A and 4C and Tab G in S1 Table). The average area of living plant tissue was quantified after 12 days of growth. Plant lines which grew significantly larger than Tak-1 and Tak-2 plants on thaxtomin A were classed as resistant.

The 17 predicted loss-of-function Mp*rtn4ip1l* lines were significantly larger than both Tak-1 and Tak-2 on 5 μM thaxtomin A so were classed as thaxtomin A-resistant ($p<0.05$) (Fig 4B). The 2 mutants with small in frame indels in Mp*rtn4ip1l* and the lines with a wild type copy of Mp*RTN4IP1L* however did not grow significantly larger than Tak-1 and Tak-2 on 5 μM thaxtomin A so were classed as thaxtomin A-sensitive (Fig 4B). This suggests that loss-of-function of Mp*RTN4IP1L* confers resistance to thaxtomin A.

When grown in control conditions, the areas of plant lines with a wild type copy of Mp*RTN4IP1L* and the 2 Mp*rtn4ip1l* mutants with small in frame indels are statistically indistinguishable from wild type (Fig 4C). However, 13 of the 17 predicted loss-of-function Mp*rtn4ip1l* mutants were significantly smaller than wild type lines in control conditions (Fig 4C). Loss-of-function of Mp*RTN4IP1L* therefore likely causes decreased growth in control conditions.

To quantify the thaxtomin A resistance of Mp*rtn4ip1l* CRISPR mutants, gemmae from 2 independent Mp*rtn4ip1l* CRISPR lines (Mp*rtn4ip1l*^{GE118} and Mp*rtn4ip1l*^{GE149}) were grown on solid medium supplemented with different doses of thaxtomin A (Fig 4D). The average area of living plant tissue was quantified after 12 days of growth (Tab H in S1 Table). Dose-response curves were fitted using the four-parameter log-logistic equation (Fig 4D). Three parameters of resistance were calculated from the curves: IC_{50} (the concentration of thaxtomin A at which the area of living tissue is reduced by 50%), LD_{100} (lethal dose at which there is no surviving tissue), and RI (resistance index; ratio between wild type and mutant IC_{50}). The IC_{50} of Tak-2 was used to calculate the most conservative estimate of RI of each Mp*rtn4ip1l* line. The IC_{50}, RI, and LD_{100} values of both Mp*rtn4ip1l* mutant lines were significantly higher than either wild type line (Fig 4D). Based on their RI, Mp*rtn4ip1l*^{GE118} and Mp*rtn4ip1l*^{GE149} are respectively at least 9.1 ± 2.95 times and 4.1 ± 2.29 times more resistant to thaxtomin A than wild type (Fig 4D). Taken together, these data indicate that loss-of-function mutations in Mp*RTN4IP1L* confer thaxtomin A resistance.

Mp*rtn4ip1l* mutants produce lower levels of coenzyme Q and accumulate higher levels of reactive oxygen species than wild type plants

Having shown that loss-of-function mutations in the Mp*RTN4IP1L* gene confer thaxtomin A resistance, we sought to determine how these mutations changed the physiology of plants to make them thaxtomin A resistant. HsRTN4IP1 interacts with proteins involved in coenzyme Q (CoQ) synthesis and knock-out mutants in the mouse *RTN4IP1* gene accumulate less CoQ than wild type [42]. We therefore hypothesized that CoQ levels would be lower in Mp*rtn4ip1l* mutants than in wild type *M. polymorpha*. To test this hypothesis, we measured the levels of coenzyme Q10 (CoQ) in the extracts of wild type (Tak-1) and Mp*rtn4ip1l*^{GE149} mutants via LC-MS/MS. The levels of CoQ in Mp*rtn4ip1l*^{GE149} are significantly lower than wild type levels in both control and TXTA-treated conditions, consistent with the hypothesis that Mp*RTN4IP1L* is involved in CoQ synthesis (Fig 5A and Tab I in S1 Table).

Coenzyme Q is an electron acceptor that transports electrons from Complexes I and II to Complex III of the oxidative phosphorylation electron transport chain [46]. As electrons flow through the electron transport chain, electrons may leak from Complexes I, II and III and react with oxygen to form reactive oxygen species (ROS). The binding site of CoQ at Complex I is one of the sites of ROS production in the mitochondria [46]. Reduced levels of CoQ result

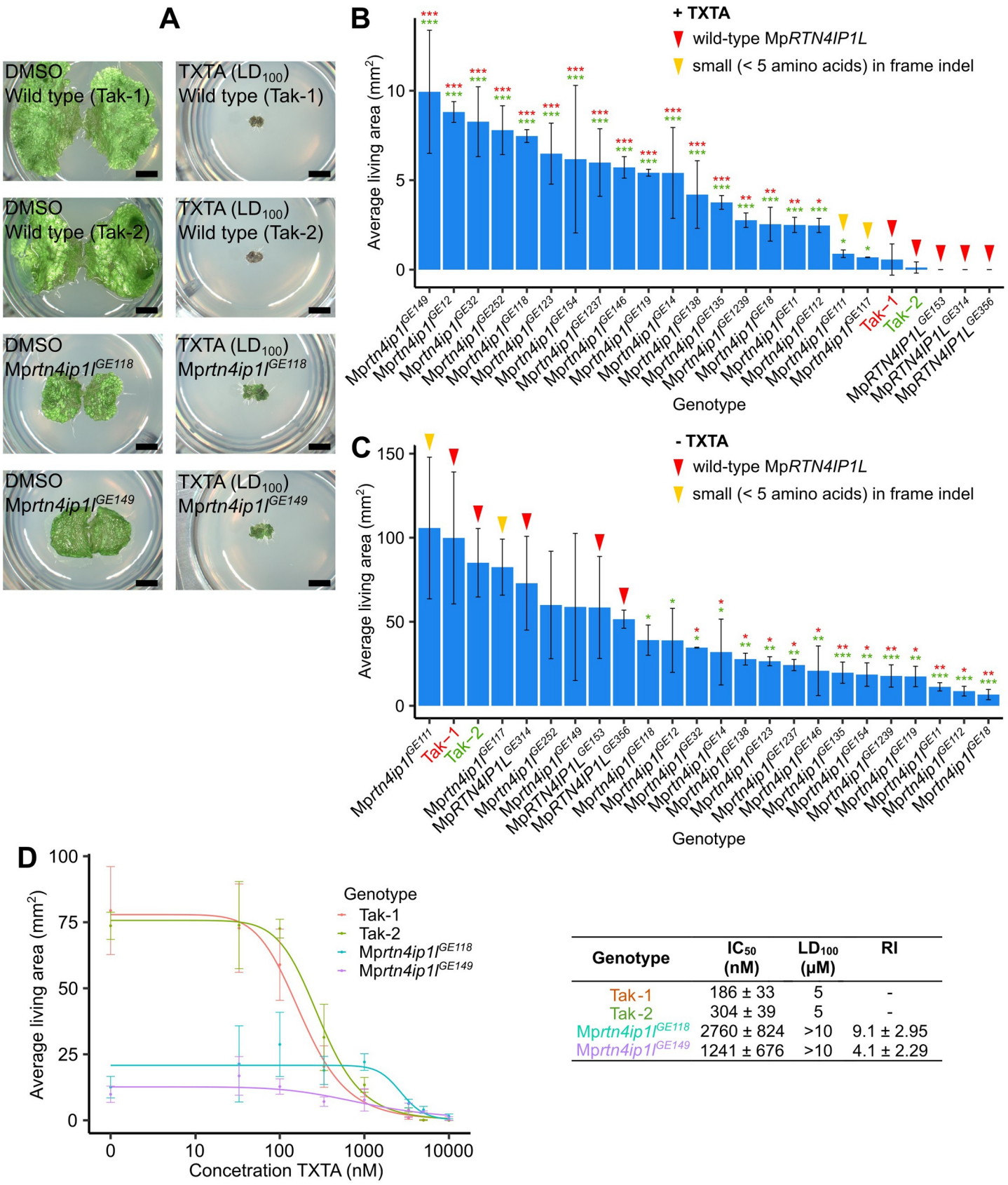

Genotype	IC_{50} (nM)	LD_{100} (μM)	RI
Tak-1	186 ± 33	5	-
Tak-2	304 ± 39	5	-
Mp*rtn4ip1l*^{GE118}	2760 ± 824	>10	9.1 ± 2.95
Mp*rtn4ip1l*^{GE149}	1241 ± 676	>10	4.1 ± 2.29

Fig 4. Loss-of-function of Mp*RTN4IP1L* confers resistance to thaxtomin A. A: Gemmae from wild type lines (Tak-1 and Tak-2) and from Mp*rtn4ip1l* mutants (Mp*rtn4ip1l*^{GE118} and Mp*rtn4ip1l*^{GE149}) were grown for 12 days on solid medium supplemented with DMSO or 5 μM thaxtomin A (TXTA). Images were taken with a Keyence VHX-7000 and the maximum pixel value was adjusted to 200 in ImageJ. Scale bars represent 2 mm and were added in Inkscape v1.0.1. **B and C:** Wild type gemmae (Tak-1 and Tak-2) and gemmae from Mp*rtn4ip1l* mutants were grown for 12 days on solid medium supplemented with 5 μM thaxtomin A (**B**) (Tab F in S1 Table) or 0.1% DMSO (**C**) (Tab G in S1 Table). Error bars represent ± standard deviation (n = 2–6). Stars represent the level of significance (as determined by Student's t-tests) of the difference between mutant and control lines (comparison to Tak-1 in red and Tak-2 in green): * = $p < 0.05$, ** = $p < 0.01$, *** = $p < 0.001$. Red arrowheads indicate lines with a wild type copy of Mp*RTN4IP1L*; yellow arrowheads indicate lines with a small (< 5 amino acids) in frame indel in Mp*RTN4IP1L*. Arrowheads were added in Inkscape v1.0.1. **D:** Dose-response curves of the growth of wild type and Mp*rtn4ip1l* mutants on thaxtomin A, and table of corresponding IC_{50}, LD_{100}, and RI values. Gemmae from wild type lines (Tak-1 and Tak-2) and from two independent Mp*rtn4ip1l* mutants generated via CRISPR-Cas9 mutagenesis (Mp*rtn4ip1l*^{GE118} and Mp*rtn4ip1l*^{GE149}) were grown for 12 days on solid medium supplemented with different concentrations of thaxtomin A (Tab H in S1 Table). The fitted curves and IC_{50} values were calculated using the four-parameter log-logistic equation. Error bars represent ± standard deviation (n = 3).

https://doi.org/10.1371/journal.pgen.1010423.g004

in fewer electron carriers active in the oxidative phosphorylation transport chain leading to an excess of electrons leaking from the chain and reacting with oxygen to form ROS. Furthermore, non-mitochondrial CoQ acts as a lipid soluble antioxidant, protecting against oxidative stress by reacting with lipid peroxide radicals thereby preventing their ability to cause lipid peroxidation [47–49]. Therefore, we hypothesized that ROS levels would be higher in Mp*rtn4ip1l* mutants than in wild type plants.

To test the hypothesis that Mp*rtn4ip1l* mutants produce higher levels of ROS than wild type plants, 12-day old gemmalings of Tak-1, Tak-2, Mp*rtn4ip1l*^{GE118} and Mp*rtn4ip1l*^{GE149} were stained with 3,3'-diaminobenzidine (DAB). DAB reacts with hydrogen peroxide (H_2O_2)–a form of ROS–to form a brown precipitate. The amount of brown precipitate is proportional to the amount of H_2O_2 in each sample [50]. The two Mp*rtn4ip1l* mutants stained darker than the two wild type lines, indicating higher levels of H_2O_2 in mutant thalli than in wild type (Fig 5B). The concentration of various forms of ROS (including H_2O_2 and lipid hydroperoxides) was also quantified in Mp*rtn4ip1l* mutants using a modified ferric-xylenol orange (FOX) assay [51,52]. ROS concentrations were significantly higher in Mp*rtn4ip1l*^{GE118} and Mp*rtn4ip1l*^{GE149} than in wild type plants (Fig 5C and Tab J in S1 Table).

Since Mp*rtn4ip1l* mutants produce more ROS than wild type, we hypothesized that Mp*rtn4ip1l* mutants would be more sensitive (hypersensitive) to ROS treatment than wild type plants. To test this hypothesis the sensitivity of Mp*rtn4ip1l* mutants to toxic levels of exogenous ROS was compared to that of wild type plants. Furthermore, a number of herbicides including paraquat, protoporphyrinogen oxidase inhibitors and glufosinate control weeds, at least in part, by causing ROS overproduction [53–56]. Mp*rtn4ip1l* mutants produce more ROS than wild type, therefore we hypothesized that Mp*rtn4ip1l* mutants would be hypersensitive to herbicides that cause ROS overproduction.

To test the hypothesis that Mp*rtn4ip1l* mutants are more sensitive to ROS than wild type, the sensitivity of Mp*rtn4ip1l* mutants and wild type was compared. Tak-1, Tak-2, Mp*rtn4ip1l*^{GE118} and Mp*rtn4ip1l*^{GE149} gemmae were grown on solid medium supplemented with a range of concentrations of H_2O_2 or paraquat. The average area of living plant tissue was quantified after 10 days of growth (Tabs K and L in S1 Table). Dose-response curves were fitted using the four-parameter log-logistic equation, and resistance parameters IC_{50}, LD_{100} and RI were calculated from the curves (Fig 5D and 5E). Both Mp*rtn4ip1l* mutants were more sensitive to H_2O_2 than wild type lines. The RI values of Mp*rtn4ip1l*^{GE118} and Mp*rtn4ip1l*^{GE149} were 0.64 ± 0.26 and 0.88 ± 0.35 respectively, demonstrating that these lines are more sensitive to H_2O_2 than either wild type line. The RI value of Mp*rtn4ip1l*^{GE118} was statistically significant (Fig 5D). While the RI value of Mp*rtn4ip1l*^{GE1549} was not statistically significant, the LD_{100} of Mp*rtn4ip1l*^{GE149} was lower than either wild type line (Fig 5D). These data demonstrate that Mp*rtn4ip1l* mutants are more sensitive to H_2O_2 than wild type plants. Both Mp*rtn4ip1l* mutants were also more sensitive to paraquat than wild type plants. The LD_{100} of

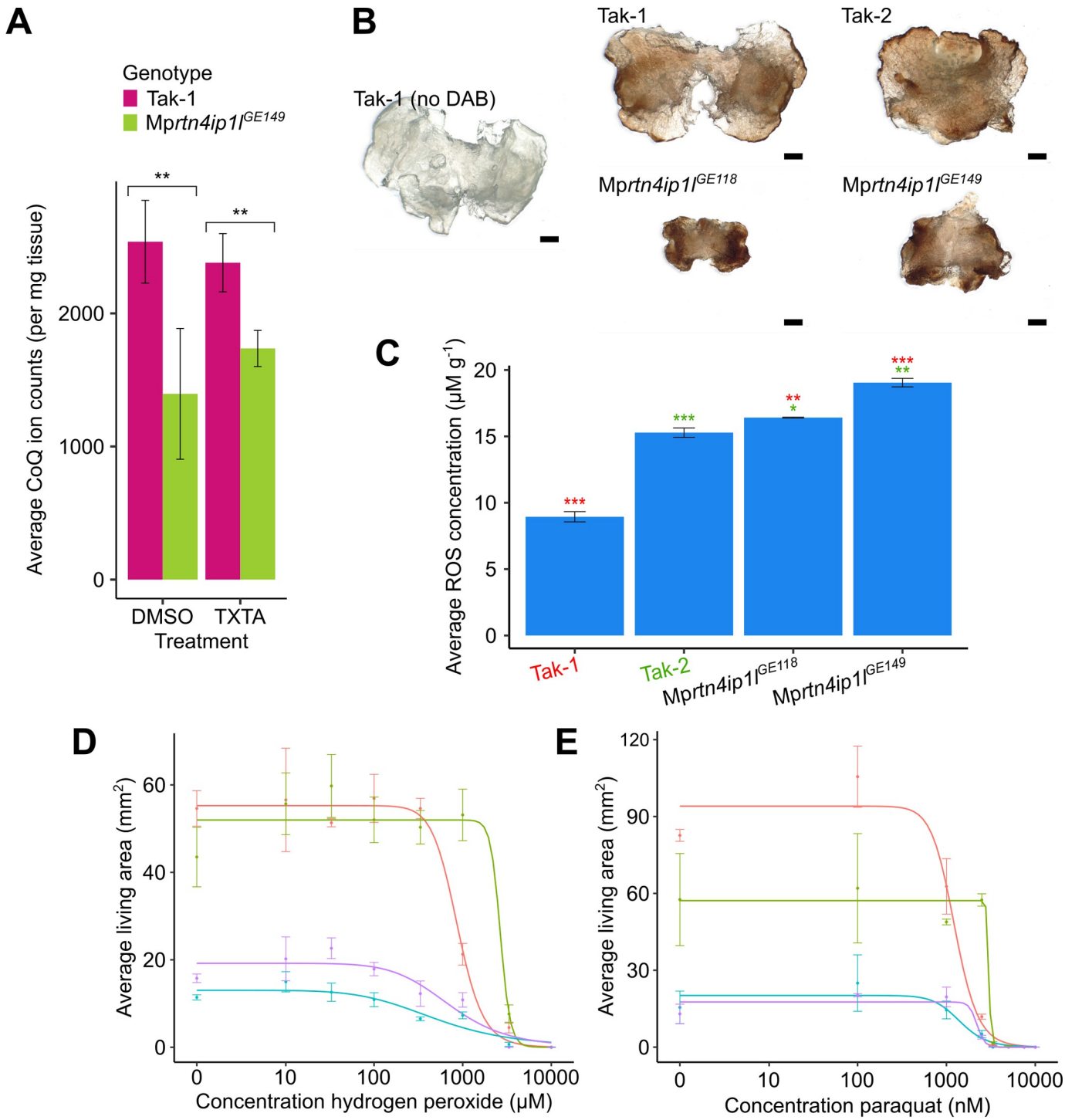

Genotype	IC_{50} (µM)	LD_{100} (mM)	RI
Tak-1	883 ± 101	10	-
Tak-2	2708 ± 2499	10	-
Mprtn4ip1l^{GE118}	567 ± 223	10	0.64 ± 0.26
Mprtn4ip1l^{GE149}	777 ± 297	3.3	0.88 ± 0.35

IC_{50} (nM)	LD_{100} (µM)	RI
1252 ± 115	7.5	-
3086 ± 2322	7.5	-
1443 ± 693	3.3	1.15 ± 0.56
2219 ± 1584	5	1.77 ± 0.85

Fig 5. Mp*rtn4ip1l* mutants are defective in coenzyme Q synthesis and overproduce reactive oxygen species. A: Ion counts of coenzyme Q10 (CoQ) in wild-type and Mp*rtn4ip1l* mutants as quantified by targeted LC-MS/MS (Tab I in S1 Table). Tak-1 and Mp*rtn4ip1l*^{GE149} gemmae were grown on solid medium supplemented with 0.1% DMSO for 14 days, then transferred to solid medium supplemented with 0.1% DMSO or 5 μM thaxtomin A for 2 days. Cellular fractions were extracted from the plants and analysed via LC-MS/MS. Stars represent the level of significance of the difference between Tak-1 and Mp*rtn4ip1l*^{GE149} samples as determined by Student's t-tests: * = $p < 0.05$, ** = $p < 0.01$, *** = $p < 0.001$. Error bars represent ± standard deviation (n = 3–6). **B:** DAB staining of Tak-1, Tak-2, Mp*rtn4ip1l*^{GE118}, and Mp*rtn4ip1l*^{GE149}. 12-day old gemmalings were stained with 3,3'- diaminobenzidine (DAB), which forms a brown precipitate upon reaction with H_2O_2. Stained plants were bleached to remove chlorophyll and imaged with a Keyence VHX-7000. Scale bars represent 500 μm and were added in Inkscape v1.0.1. **C:** Concentration of ROS in wild type and Mp*rtn4ip1l* mutants. The concentration of ROS in 12-day old Tak-1, Tak-2, Mp*rtn4ip1l*^{GE118}, and Mp*rtn4ip1l*^{GE149} plants was determined by homogenising frozen samples in perchloric acid, followed by incubation with ferric xylenol-orange (FOX) and measurement of absorbance at 560 nm using an Ultrospec 3100 pro spectrophotometer. The absorbance measurements were converted to concentrations of ROS using a calibration curve (Tab J in S1 Table). Stars represent the level of significance of the difference between mutant and control lines (Tak-1 in red and Tak-2 in green) as determined by Student's t-tests: * = $p < 0.05$, ** = $p < 0.01$, *** = $p < 0.001$. Error bars represent ± standard deviation (n = 3). **D and E:** Dose-response curves of the growth of wild type and Mp*rtn4ip1l* mutants on H_2O_2 (D) and paraquat (E). Gemmae from Tak-1 (orange), Tak-2 (green), Mp*rtn4ip1l*^{GE118} (blue), and Mp*rtn4ip1l*^{GE149} (purple) were grown for 10 days on solid medium supplemented with different concentrations of H_2O_2 (D) (Tab K in S1 Table) or paraquat (E) (Tab L in S1 Table). The fitted curves and IC_{50} values were calculated using the four-parameter log-logistic equation. Error bars represent ± standard deviation (n = 3). LD_{100} is the lowest concentration at which area of all replicates was 0. RI is the ratio between each Mp*rtn4ip1l* mutant's IC_{50} and the IC_{50} of Tak-1, the more sensitive wild type line, to calculate the most conservative estimate of RI.

https://doi.org/10.1371/journal.pgen.1010423.g005

Mp*rtn4ip1l*^{GE118} and Mp*rtn4ip1l*^{GE149} were 3.3 μM and 5 μM respectively, which are both lower than 7.5 μM, the LD_{100} of Tak-1 and Tak-2 wild types (Fig 5E). Neither of the RI values of Mp*rtn4ip1l*^{GE118} and Mp*rtn4ip1l*^{GE149} were statistically significant. Based on their LD_{100} values, Mp*rtn4ip1l* mutants are more sensitive to paraquat than wild type plants. Since paraquat kills plants by increasing ROS to toxic levels, these data demonstrate that Mp*rtn4ip1l* mutants are more sensitive to ROS than wild type plants.

Together, these data indicate that ROS levels are higher in Mp*rtn4ip1l* mutants than in wild type plants. Addition of H_2O_2 to *A*. *thaliana* cells in culture confers partial thaxtomin A resistance [57]. The stiffening of the cell wall observed upon H_2O_2 treatment is thought to prevent the toxic action of thaxtomin A on cell wall biosynthesis [57]. We hypothesize that the reduced levels of CoQ in Mp*rtn4ip1l* mutants causes thaxtomin A resistance by increasing ROS levels which changes the physiology of the plant cell walls making thaxtomin A less effective. According to this hypothesis of ROS-induced cell wall alteration, loss-of-function of Mp*rtn4ip1l* is a mechanism of non-target site resistance.

Loss-of-function of Mp*RTN4IP1L* likely confers non-target site resistance

To test the hypothesis that loss-of-function of *RTN4IP1L* results in non-target site resistance, the strength of thaxtomin A resistance and the cross resistance to other herbicides were tested in Mp*rtn4ip1l* mutants. Herbicide cross resistance and weak thaxtomin A resistance would be consistent with the hypothesis that *RTN4IP1L* loss-of-function mutations confer non-target site resistance.

The strength of thaxtomin A resistance in Mp*rtn4ip1l* mutants was measured and compared to the strength of resistance to chlorsulfuron in chlorsulfuron target-site resistant mutants. Chlorsulfuron is a herbicide which targets the enzyme acetohydroxyacid synthase (AHAS), also known as acetolactate synthase (ALS). We generated 5 *M*. *polymorpha* chlorsulfuron-resistant target-site resistant mutants–Mp*ahas*$^{chlorsulfuron\ resistant}$ (Mp*ahas*^{chlr})–in a UV-B mutagenesis screen for resistance to chlorsulfuron. Each mutant carries a target-site resistance mutation in Mp*AHAS* which confers chlorsulfuron resistance (S5 Fig). Mutations causing a Pro197Ser or Pro197Leu amino acid change, which have been observed to confer chlorsulfuron resistance in angiosperm weeds, were present in 4 out of the 5 Mp*ahas*^{chlr} mutants isolated in this screen [2,58,59].

To compare the strength of herbicide resistance in Mp*rtn4ip1l* and Mp*ahas*^{chlr} lines, gemmae from 2 independent Mp*rtn4ip1l* mutants (Mp*rtn4ip1l*^{GE118} and Mp*rtn4ip1l*^{GE149}) were grown on solid medium supplemented with LD_{100} or 5 x LD_{100} of thaxtomin A (Fig 6A and 6B), and

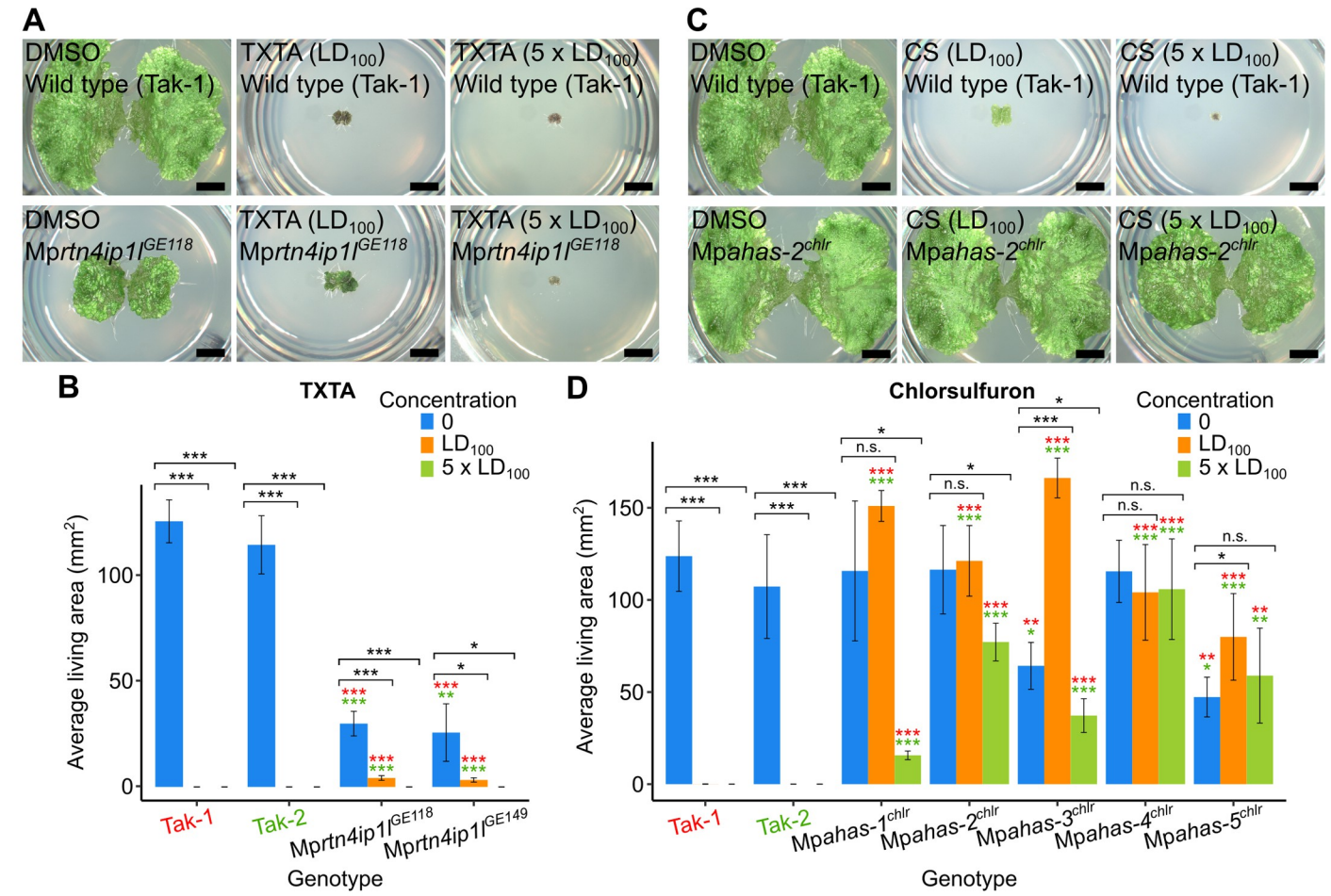

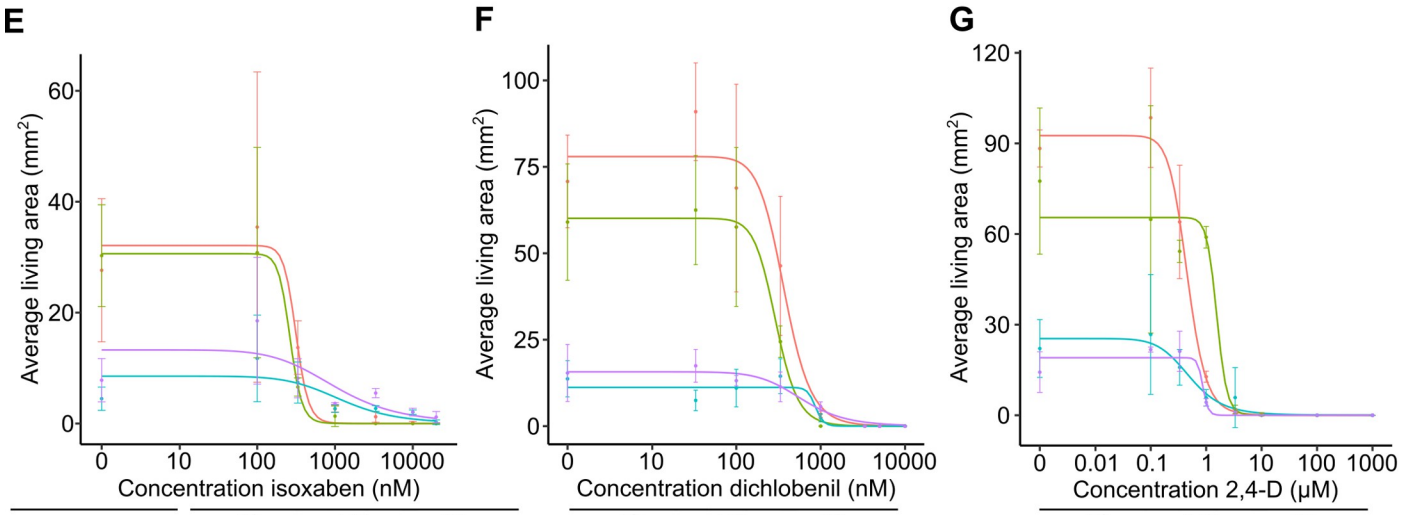

Genotype	IC_{50} (nM)	LD_{100} (μM)	RI
Tak-1	324 ± 136	20	-
Tak-2	292 ± 848	10	-
Mp*rtn4ip1l*^{GE118}	1370 ± 2850	>20	4.22 ± 8.96
Mp*rtn4ip1l*^{GE149}	1275 ± 1870	>20	3.94 ± 6.01

IC_{50} (nM)	LD_{100} (μM)	RI
367 ± 41	3.3	-
293 ± 43	1	-
886 ±1480	3.3	2.41 ± 4.04
603 ± 490	3.3	1.64 ± 1.35

IC_{50} (nM)	LD_{100} (μM)	RI
467 ± 52	100	-
1600 ± 406	100	-
523 ± 293	10	0.33 ± 0.20
892 ± 1340	100	0.56 ± 0.85

Fig 6. Loss-of-function of Mp*RTN4IP1L* likely confers non-target site resistance. A and B: Wild type gemmae (Tak-1 and Tak-2) and gemmae from Mp*rtn4ip1l* mutants were grown on solid medium supplemented with LD_{100} (5 μM) or 5 x LD_{100} (25 μM) of thaxtomin A (Tab M in S1 Table). **(A)** Gemmalings were imaged using a Keyence VHX-7000. Scale bars represent 2 mm and were added in Inkscape v1.0.1. **(B)** Error bars represent ± standard deviation (n = 3). Stars represent the level of significance (as determined by Student's t-tests) of the difference between mutant and control lines (comparison to Tak-1 in red and Tak-2 in green), or between individuals of the same genotype subjected to different treatments (black): * = $p < 0.05$, ** = $p < 0.01$, *** = $p < 0.001$. **C and D:** Wild type gemmae (Tak-1 and Tak-2) and gemmae from Mp*ahas*^{chlr} mutants were grown on solid medium supplemented with LD_{100} (33 nM) or 5 x LD_{100} (165 nM) of chlorsulfuron (Tab N in S1 Table). **(C)** Gemmalings were imaged using a Keyence VHX-7000. Scale bars represent 2 mm and were added in Inkscape v1.0.1. **(D)** Error bars represent ± standard deviation (n = 3). Stars represent the level of significance (as determined by Student's t-tests) of the difference between mutant and control lines (comparison to Tak-1 in red and Tak-2 in green), or between individuals of the same genotype subjected to different treatments (black): * = $p < 0.05$, ** = $p < 0.01$, *** = $p < 0.001$. **E,F, and G:** Dose-response curves of the growth of Mp*rtn4ip1l* mutants on herbicides with different targets and tables of corresponding IC_{50}, LD_{100}, and RI values. Gemmae from Tak-1 (orange), Tak-2 (green), Mp*rtn4ip1l*^{GE118} (blue), and Mp*rtn4ip1l*^{GE149} (purple) were grown for 12 days on solid medium supplemented with different doses of isoxaben (**E**) (Tab O in S1 Table), dichlobenil (**F**) (Tab P in S1 Table), or 2,4-D (**G**) (Tab Q in S1 Table). The fitted curves and IC_{50} values were calculated using the four-parameter log-logistic equation. Error bars represent ± standard deviation (n = 3). LD_{100} is the lowest concentration at which area of all replicates was 0. RI was calculated as the ratio between each Mp*rtn4ip1l* mutant's IC_{50} and the IC_{50} of the most resistant wild type line to calculate the most conservative estimate of RI.

https://doi.org/10.1371/journal.pgen.1010423.g006

gemmae from 5 independent Mp*ahas*^{chlr} mutant lines were grown on solid medium supplemented with LD_{100} or 5 x LD_{100} of CS (Fig 6C and 6D). The average area of living plant tissue was quantified after 12 days of growth (Tabs M and N in S1 Table).

Mp*rtn4ip1l* mutants are significantly larger than wild type plants on the thaxtomin A LD_{100}, confirming their thaxtomin A resistance (Fig 6A and 6B). Similarly, Mp*ahas*^{chlr} mutants are significantly larger than wild type on the chlorsulfuron LD_{100} (Fig 6C and 6D). However, Mp*rtn4ip1l* mutants grow significantly less on thaxtomin A LD_{100} than in control conditions (Fig 6A and 6B). Conversely, Mp*ahas*^{chlr} mutants are either statistically indistinguishable or significantly larger when grown on chlorsulfuron LD_{100} than in control conditions (Fig 6C and 6D). This suggests that Mp*rtn4ip1l* mutants are weakly resistant to thaxtomin A, whereas Mp*ahas*^{chlr} mutants are strongly resistant to chlorsulfuron. This is consistent with the hypothesis that Mp*rtn4ip1l* mutants are non-target site resistant.

Mp*rtn4ip1l* mutants die when grown on five times the LD_{100} of thaxtomin A (Fig 6A and 6B), whereas Mp*ahas*^{chlr} mutants do not die on five times the LD_{100} of chlorsulfuron (Fig 6C and 6D). The inability of Mp*rtn4ip1l* mutants to survive 5 x LD_{100} is also consistent with the hypothesis that Mp*rtn4ip1l* mutants are weakly resistant to thaxtomin A. Resistance from loss-of-function mutations in Mp*rtn4ip1l* is therefore more likely to be non-target site resistance than target-site resistance.

To further test the hypothesis that loss-of-function of Mp*rtn4ip1l* function causes non-target site resistance against thaxtomin A, we tested if Mp*rtn4ip1l* mutants were resistant to other herbicides (cross resistance). To quantify the cross resistance of Mp*rtn4ip1l* mutants to different herbicides, the resistance of Mp*rtn4ip1l*^{GE118} and Mp*rtn4ip1l*^{GE149} to the herbicides isoxaben, dichlobenil, and 2,4-D was tested. Isoxaben targets cellulose biosynthesis, targeting the cellulose synthase subunits CESA1, CESA3, and CESA6 [60]. Dichlobenil is also classed as a cellulose biosynthesis inhibitor, but its target protein is still unknown [61]. 2,4-D is an auxin mimic, causing deregulation of the auxin signalling pathway [62]. Gemmae from Tak-1, Tak-2, Mp*rtn4ip1l*^{GE118}, and Mp*rtn4ip1l*^{GE149} were grown on solid medium supplemented with different doses of isoxaben (Fig 6E), dichlobenil (Fig 6F), or 2,4-D (Fig 6G). After 10 days of growth, the area of living tissue was quantified (Tabs O, P, and Q in S1 Table), and dose-response curves were fitted using the four-parameter log-logistic equation. IC_{50}, LD_{100}, and RI for wild type and Mp*rtn4ip1l* mutant lines were calculated from the resulting dose-response curves (Fig 6E, 6F and 6G).

Mp*rtn4ip1l* mutant lines were resistant to isoxaben, Mp*rtn4ip1l*^{GE118} with an RI of 4.22 ± 8.96 and Mp*rtn4ip1l*^{GE149} with an RI of 3.94 ± 6.01. Although these RI values are not statistically significant, the LD_{100} of both Mp*rtn4ip1l* mutant lines was higher than wild type; both were alive when grown on 20 μM isoxaben which is lethal to Tak-1 and Tak-2 (Fig 6E).

These data demonstrate that Mp*rtn4ip1l*^{GE118} and Mp*rtn4ip1l*^{GE149} are resistant to isoxaben. The cross resistance of Mp*rtn4ip1l* mutants to isoxaben is consistent with the hypothesis that loss of Mp*RTN4IP1L* function confers non-target site resistance.

Mp*rtn4ip1l* mutant lines were not resistant to dichlobenil or 2,4-D. The RI values of Mp*rtn4ip1l*^{GE118} and Mp*rtn4ip1l*^{GE149} on dichlobenil are not statistically significant, and neither mutant can survive at a higher concentration of dichlobenil than wild type (Fig 6F). Mp*rtn4ip1l*^{GE118} has an RI value of 0.33 ± 0.20 on 2,4-D so is significantly 2,4-D sensitive, while the RI of Mp*rtn4ip1l*^{GE149} on 2,4-D is not statistically significant. Neither Mp*rtn4ip1l* mutant has a higher LD_{100} than wild type on 2,4-D (Fig 6G). Mp*rtn4ip1l* lines are therefore not cross resistant to dichlobenil or 2,4-D.

Taken together, the weak thaxtomin A resistance and isoxaben cross resistance of Mp*rtn4ip1l* mutants demonstrate that loss-of-function of Mp*RTN4IP1L* is likely to confer non-target site resistance. It is possible that this non-target site resistance results from ROS-induced alterations to the cell wall that reduce the effect of thaxtomin A. Non-target site resistance is however often caused by chemical modification of a herbicide resulting in the formation of a non-toxic product, or by reduced herbicide uptake [1,6]. Therefore, an alternative hypothesis to the ROS-induced cell wall alteration hypothesis is that non-target site resistance to thaxtomin A in Mp*rtn4ip1l* mutants is caused by a change in herbicide metabolism or uptake.

Mp*rtn4ip1l* mutants are defective in thaxtomin A metabolism

We set out to test the hypothesis that non-target site resistance in Mp*rtn4ip1l* mutants results from differences in the metabolism or uptake of thaxtomin A between wild type and mutants. To test this hypothesis, thaxtomin A and putative thaxtomin A metabolites in thaxtomin A-treated samples of Tak-2 wild type and Mp*rtn4ip1l*^{GE118} mutants were detected via a precursor ion analysis for the two most abundant fragment ions of thaxtomin A using LC/MS-MS (Fig 7A and 7B). There is a peak of pure thaxtomin A (retention time–RT– 8.99 min) and a peak of an unknown compound (RT 9.25 min) in the chromatogram of wild type Tak-2 (Fig 7A). Both peaks are absent in the analysis of the untreated samples (S6A Fig). The two prominent fragment ions of thaxtomin A are present in the MS/MS spectra of the unknown compound, suggesting that it is a thaxtomin A derivative (S6B and S6C Fig). The molecular mass of the unknown compound is 45 Da less than pure thaxtomin A. An explanation for these observations is that the unknown compound is a derivative of thaxtomin A that lacks the NO_2 group (delta mass of 45 Da) (Fig 7C and 7D). This suggests that wild type *M. polymorpha* metabolizes thaxtomin A by removing the NO_2 group of the 4-nitro-tryptophan moiety. These two peaks are present in the chromatogram from Mp*rtn4ip1l*^{GE149}. However, the RT 9.25 peak is considerably smaller in Mp*rtn4ip1l*^{GE149} than wild type (Fig 7B). This suggests that Mp*rtn4ip1l* mutants accumulate less of the derivative and are therefore defective in thaxtomin A metabolism.

To quantify the potential defect in thaxtomin A metabolism in Mp*rtn4ip1l* mutants, we measured the relative amounts of thaxtomin A (RT 8.99) and the putative thaxtomin A derivative (RT 9.25 min) in wild type and mutant plants using targeted LC-MS/MS employing selected reaction monitoring (Fig 7E and 7F, and Tabs R and S in S1 Table). The concentration of thaxtomin A is significantly higher in Mp*rtn4ip1l*^{GE118} than in Tak-2 ($p < 0.05$) (Fig 7E). This is consistent with the hypothesis that the chemical modification of thaxtomin A is defective in the mutants (Fig 7E). Furthermore, this is inconsistent with the hypothesis that Mp*rtn4ip1l* mutants uptake less thaxtomin A than wild type plants, suggesting that their resistance is not conferred by reduced herbicide uptake.

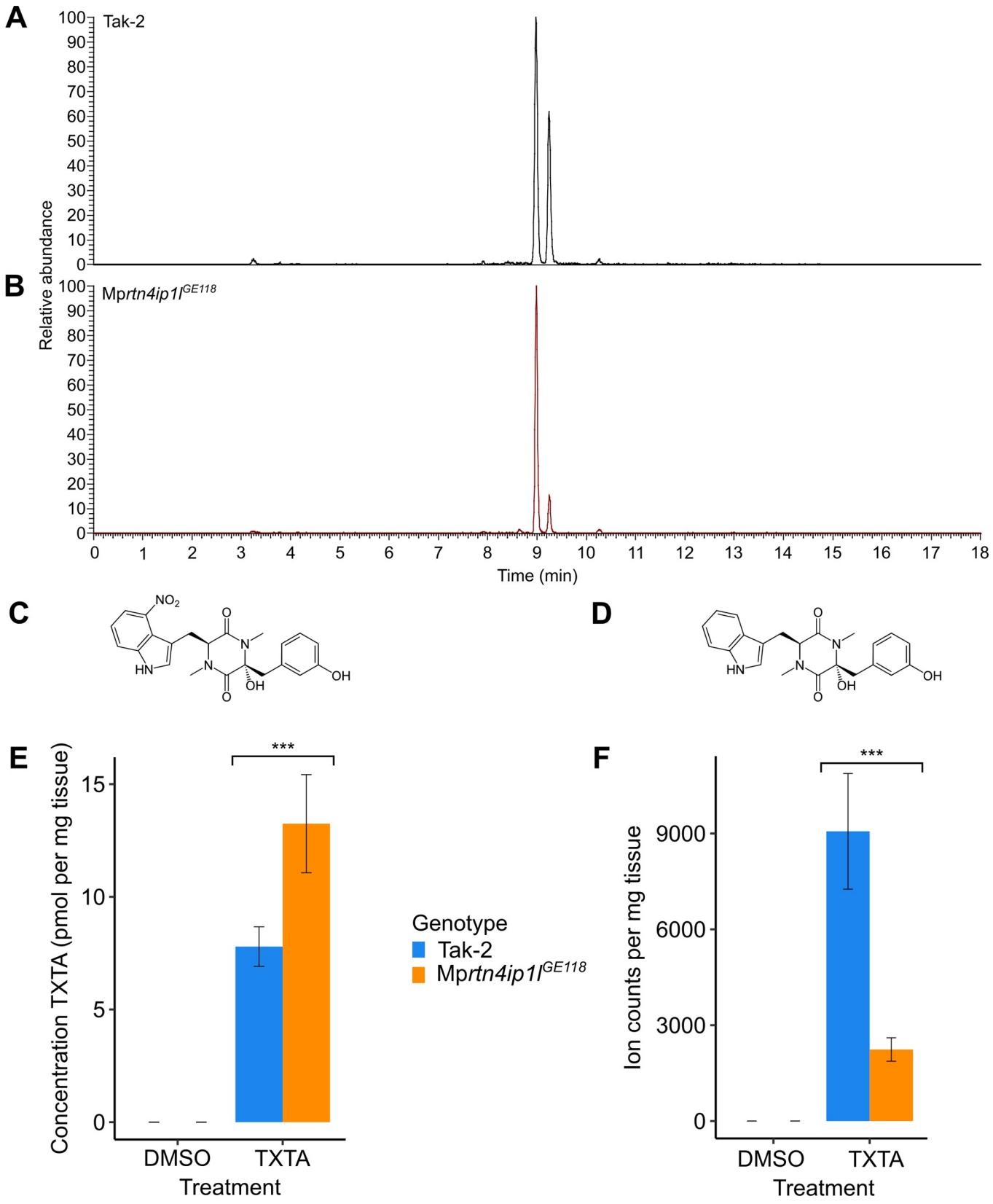
A
Tak-2
B
Mprtn4ip1l^GE118
Relative abundance
Time (min)
C
D
E
Concentration TXTA (pmol per mg tissue)
***
DMSO
TXTA
Treatment
Genotype
Tak-2
Mprtn4ip1l^GE118
F
Ion counts per mg tissue
***
DMSO
TXTA
Treatment

Fig 7. Mp*rtn4ip1l* mutants are defective in thaxtomin A metabolism. A and B: LC-MS/MS analysis of thaxtomin A and its putative metabolite in Tak-2 **(A)** and Mp*rtn4ip1l*^{GE118} **(B)** extracts. Gemmae from each line were grown on solid medium supplemented with 0.1% DMSO for 14 days, then transferred to solid 1 medium supplemented with 5 μM thaxtomin A and grown for 2 days. Cellular fractions were extracted from thaxtomin A-treated samples and a precursor ion analysis was conducted via LC-MS/MS (n = 6). Chromatograms of the total ion currents of precursor ion scanning for *m/z* 247.1 are depicted. The peak eluting at a retention time of 8.99 min. is thaxtomin A (*m/z* 439.1), the peak eluting at a retention time of 9.25 (*m/z* 394.1) is its putative metabolite. **C:** Molecular structure of thaxtomin A **D:** Molecular structure of putative thaxtomin A metabolite **E:** Concentration of pure thaxtomin A (TXTA) in DMSO and herbicide-treated samples of Tak-2 and Mp*rtn4ip1l*^{GE118} as quantified by targeted LC/MS-MS (Tab R in S1 Table). **F:** Ion counts (normalised by weight) of the putative thaxtomin A metabolite in DMSO and herbicide-treated samples of Tak-2 and Mp*rtn4ip1l*^{GE118} as quantified by targeted LC-MS/MS (Tab S in S1 Table).

https://doi.org/10.1371/journal.pgen.1010423.g007

The ion counts of the putative thaxtomin A derivative (RT 9.25) are significantly lower in Mp*rtn4ip1l*^{GE118} than in Tak-2 ($p < 0.05$), consistent with the hypothesis that the chemical modification of thaxtomin A is defective in the mutants (Fig 7F). Although the difference in the concentration of thaxtomin A between the samples cannot be directly compared to the difference in ion counts of the unknown compound, these data suggest that wild type plants metabolize thaxtomin A to form a derivative compound, but this metabolism is defective in Mp*rtn4ip1l* mutants. Given that Mp*rtn4ip1l* mutants are resistant to thaxtomin A, this is consistent with the hypothesis that thaxtomin A metabolism has a toxic effect on the plant.

To independently verify that the metabolism of thaxtomin A is defective in Mp*rtn4ip1l* mutants, the presence of thaxtomin A and its putative metabolite were also detected via precursor ion analysis in Tak-1 wild type and Mp*rtn4ip1l*^{GE149} mutants. The peak corresponding to the putative metabolite was stronger in Tak-1 than in Mp*rtn4ip1*^{GE149}, supporting the hypothesis that thaxtomin A metabolism is defective in Mp*rtn4ip1* mutants (S6D Fig).

Together these data indicate that a thaxtomin A derivative that accumulates in wild type plants accumulates at much lower levels in the resistant Mp*rtn4ip1l* mutants. It is hypothesized that the metabolism of thaxtomin A is toxic to plants. According to this hypothesis, Mp*rtn4ip1l* mutants are resistant to thaxtomin A because they are defective in thaxtomin A metabolism. The high levels of ROS produced in Mp*rtn4ip1l* mutants because of low levels of CoQ may inhibit the metabolism of thaxtomin A.

Discussion

We report the discovery of a novel mechanism of non-target site resistance caused by loss-of-function mutations in the Mp*RTN4IP1L* gene using a forward genetic screen. We demonstrate that loss-of-function Mp*rtn4ip1l* mutants are resistant to thaxtomin A. Resistance is relatively weak and mutants are also cross resistant to isoxaben which suggests that the relative insensitivity to thaxtomin A is not because of a form of target-site resistance. Instead, there is evidence that thaxtomin A resistance in the Mp*rtn4ip1l* mutants is the result of non-target site resistance. Consistent with the hypothesis that the resistance is not due to target site mutation but instead an example of non-target site resistance is the observation that the mutants produce more ROS than wild type plants. Furthermore, the metabolism of thaxtomin A is different in the resistant mutants than in wild type, consistent with non-target site resistance.

While our data suggest that the resistance resulting from loss-of-function mutations in the Mp*RTN4IP1L* gene is not caused by a thaxtomin A-insensitive target, there are a number of possible mechanisms which could explain non-target site resistance in these mutants. One hypothesis to explain thaxtomin A resistance is that metabolism of the herbicide is defective in Mp*rtn4ip1l* mutants. If correct, this would be a rare instance of a decrease in herbicide metabolism conferring non-target site resistance, which is usually associated with increased metabolism [6].

If resistance were the result of defective thaxtomin A metabolism, then it is possible that thaxtomin A acts as a proherbicide. Proherbicides are non-toxic molecules that require

metabolism to form a herbicidally active, toxic molecule [63]. We demonstrated that a thaxtomin A metabolite is present at significantly lower levels in Mp*rtn4ip1l* mutants than in wild-type plants. Therefore, if thaxtomin A is a proherbicide and non-toxic, the metabolite could be toxic and consequently herbicidal. If true, the decreased thaxtomin A metabolism in Mp*rtn4ip1l* mutants would prevent the production of herbicidally active molecules that contribute to thaxtomin A non-target site resistance.

While our data are consistent with the hypothesis that thaxtomin A is a proherbicide, there is evidence that refute this hypothesis. The difference in molecular mass (45 Da) between thaxtomin A and the metabolite are consistent with the hypothesis that the metabolite lacks the NO_2 group, although this has not been verified. The NO_2 group of thaxtomin A has been shown to be required for phytotoxicity [22]. If the NO_2 group is required for phytotoxicity, and if the thaxtomin A metabolite lacks the NO_2 group, it would suggest that the observed thaxtomin A metabolite is not toxic. This would be inconsistent with thaxtomin A acting as a proherbicide. Therefore, while we propose that non-target site resistance in Mp*rtn4ip1l* mutants results from defective thaxtomin A metabolism, we have not proved that thaxtomin A acts as a proherbicide.

It is formally possible that the defective thaxtomin A metabolism observed in Mp*rtn41ipl* mutants may result from elevated levels of ROS in the mutant. Mp*rtn4ip1l* mutants are defective in the biosynthesis of coenzyme Q, an electron transporter in oxidative phosphorylation. Consequently, mutants produce more ROS than wild type plants. The increased ROS levels in Mp*rtn4ip1l* mutants may inhibit the chemical reactions involved in the metabolism of thaxtomin A observed in wild type. It is therefore possible that ROS-inhibited thaxtomin A metabolism could lead to thaxtomin A resistance.

It is also possible that high ROS levels in Mp*rtn4ip1l* mutants confer herbicide resistance by altering the properties of the cell wall. Thaxtomin A is classed as a cellulose biosynthesis inhibitor [29,30]. It is therefore possible that physiological changes to the cell wall which hinder the action of thaxtomin A could confer non-target site thaxtomin A resistance. It is well established that ROS can cause physiological changes to the cell wall, such as cell wall stiffening upon abiotic stress by cross-linking or altering cell wall proteins [57,64–67]. It is therefore possible that ROS-induced cell wall alterations could confer resistance to thaxtomin A in Mp*rtn4ip1l* mutants.

The effects of ROS and thaxtomin A on *A*. *thaliana* cell walls are consistent with the hypothesis that ROS-induced cell wall alterations could confer thaxtomin A resistance. *A*. *thaliana* cell walls stiffen upon ROS treatment but loosen upon treatment with the cellulose biosynthesis inhibitors thaxtomin A and isoxaben [57,68]. Thaxtomin A and isoxaben may therefore have antagonistic effects to ROS on the cell wall. Furthermore, ROS pretreatment prevents thaxtomin A-induced cell wall loosening and confers resistance to thaxtomin A. [57]. This suggests that ROS-induced cell wall stiffening can protect against the toxic effect of thaxtomin A. Therefore, according to the ROS-induced cell wall alteration hypothesis, increased ROS levels in Mp*rtn4ip1l* mutants cause cell wall stiffening which prevents the cell wall loosening action of thaxtomin A and isoxaben. The ROS-induced cell wall alteration hypothesis therefore also accounts for the cross-resistance of Mp*rtn4ip1l* mutants to isoxaben.

According to the ROS-induced cell wall alteration hypothesis, cross resistance of Mp*rtn4ip1l* to thaxtomin A and isoxaben would be due to the cell wall stiffening effect of ROS which counters the action of these two cellulose biosynthesis inhibitors. However, Mp*rtn4ip1l* mutants are not resistant to the cellulose biosynthesis inhibitor dichlobenil. Thaxtomin A and isoxaben are classed as group 1 cellulose biosynthesis inhibitors and dichlobenil is classed as group 2 [30]. Group 1 cellulose biosynthesis inhibitors cause depletion of cellulose synthase complexes from the plasma membrane; group 2 cellulose biosynthesis inhibitors however

cause accumulation of cellulose synthase complexes at the plasma membrane [30]. Given the opposite effects of Group 1 and Group 2 cellulose biosynthesis inhibitors on cellulose synthase enzymes, it is possible that some resistance alleles confer resistance to one group of cellulose biosynthesis inhibitors but not the other. Therefore, according to the ROS-induced cell wall alteration hypothesis, the cross-resistance pattern observed in Mp*rtn4ip1l* mutants results from ROS-induced changes to the cell wall conferring resistance to group 1 but not group 2 cellulose biosynthesis inhibitors.

The mechanism of non-target site resistance reported here is also likely to operate in angiosperm weeds and not be restricted to *M*. *polymorpha* or other liverworts. First, the *RTN4IP1L* gene is found throughout the angiosperms and therefore agricultural weeds, where mutation would likely result in resistance. Second, our data indicate that loss-of-function mutations in the *PAM16* gene confer weak thaxtomin A resistance in both *M*. *polymorpha* and *A*. *thaliana* [20]. Therefore, non-target site resistance caused by loss of *PAM16* function in *M*. *polymorpha* also operates in angiosperms, demonstrating that some mechanisms of non-target site resistance are conserved between *M*. *polymorpha* and angiosperms. Furthermore, we report that four chlorsulfuron-resistant *M*. *polymorpha* UV-B mutants carry Pro197Ser or Pro197Leu mutations, which are among the most frequently reported mechanisms of chlorsulfuron resistance observed in chlorsulfuron-resistant angiosperm weeds [2,58,59]. Together, these data demonstrate that several herbicide resistance mechanisms are conserved between *M*. *polymorpha* and angiosperms, validating the use of *M*. *polymorpha* as a model with which to identify novel mechanisms of non-target site resistance which could evolve in weeds.

Most Mp*rtn4ip1l* mutants are smaller than wild type plants in control conditions, suggesting that loss of Mp*RTN4IP1L* function would incur a considerable fitness cost in the wild. Given this, the evolution of Mp*rtn4ip1l* complete loss-of-function based resistance in the field is unlikely. However, some herbicide resistance alleles incur small fitness costs but are nevertheless maintained in weed populations due to the intense selection imposed by herbicide treatment [69–72]. We propose that weak loss-of-function alleles of *RTN4IP1L* (or mutations which affect the same molecular processes), which cause negligible or small fitness costs, could evolve in weed populations treated with thaxtomin A. If weak loss-of-function of *RTN4IP1L* is identified in resistant weeds in the field, our findings can inform weed management practices. Based on our characterization of phenotypes of Mp*rtn4ip1l* loss-of-function mutants, weeds with *RTN4IP1L* loss-of-function mutations cannot be controlled by isoxaben. However, our data suggest that weeds that evolve thaxtomin A resistance through loss-of-function mutations in the *RTN4IP1L* gene, or through the overproduction of ROS, are hypersensitive to paraquat, and are therefore likely hypersensitive to other herbicides that kill plants by ROS overproduction such as protoporphyrinogen oxidase inhibitors or glufosinate [53–56].

Our findings demonstrate the potential to identify novel mutations conferring non-target site herbicide resistance which have been difficult to identify and characterize to date. Our methodology can uncover novel mechanisms of non-target site resistance caused by loss-of-function mutations which could inform efficient weed management.

Materials and methods

Plant lines and growth conditions

Wild-type plants were *M*. *polymorpha* laboratory accessions Takaragaike-1 (Tak-1) and Takaragaike-2 (Tak-2) [73]. Mp*pam16* and Mp*rtn4ip1l* lines were generated via CRISPR-Cas9 mutagenesis of wild-type *M*. *polymorpha* spores (from a cross between Tak-1 and Tak-2). All lines were maintained via asexual propagation of gemmae or thallus excision in the case of mutants which did not produce gemmae. Plants were grown on solid ½ Gamborg medium. All plant

material used for experiments was grown in a growth chamber at 23˚C under 24-hour 10–30 μmol m^{-2} s^{-1} white light. Plant material to be stored long-term was kept in a growth chamber at 17˚C under 6 hours 10–30 μmol m^{-2} s^{-1} white light and 18 hours dark. To produce spores, plants were grown on a mixture of John Innes n. 2 compost and fine vermiculite at a ratio of 2:1. Plants were grown in growth chambers at 23˚C and under 16 hours white light and continuous far-red light to induce transition to the reproductive phase. Once mature, water was pipetted onto the antheridia produced by male plants to collect sperm, then transferred to archegonia produced by female plants. Sporangia were harvested before bursting and stored fresh at 4˚C in sterile dH_2O.

Fresh spore sterilization

Fresh sporangia were sterilized with 1% NaDCC (sodium dichloroisocyanurate) for 4 minutes followed by rinsing with sterile dH2O.

Chemicals and stock solution preparation

Thaxtomin A (TXTA) (SML1456), dichlobenil (45431), isoxaben (36138), chlorsulfuron (34322), 2,4-dichlorophenoxyacetic acid (2,4-D) (31518), and paraquat (36541) were obtained from Sigma-Aldrich. Stock solutions were prepared by dissolving in pure dimethyl sulfoxide (DMSO) (D8418) from Sigma-Aldrich.

Gemmaling dose-response assays

Gemmae were grown on solid ½ Gamborg medium supplemented with different concentrations of herbicide dissolved in DMSO (n = 2–18; see individual figure legends for experiment-specific biological replicate numbers). Gemmalings were imaged using a Berthold Nightowl II LB 983 *In Vivo* Imaging System (Berthold, Bad Wildbad, Germany). Images were taken after exposing gemmalings to 120 s white light. The imaging system detects chlorophyll autofluorescence (560 nm). The lateral area of autofluorescing (living) tissue was determined using the indiGo software package (Berthold, Bad Wildbad, Germany). Dose-response curves were generated using the ggplot2 and drc packages in R [74,75]; the four-parameter log-logistic equation with a fixed lower limit of 0 was used to fit a dose-response curve to the data.

Phylogenetic analysis of PAM16 and RTN4IP1 homologues

Homologues of the *A*. *thaliana* At3G59280 protein or of the *H*. *sapiens* RTN4IP1.1 protein were identified by protein BLAST search against the reference proteomes of various species [37]. Only homologues with an E value less than 1E-5 were used to construct the trees. Homologues were aligned via the L-INS-i strategy using MAFFT version 7 [76]. The alignments were manually trimmed using BioEdit7.2. A maximum likelihood tree was constructed with PhyML 3.0 using an estimated gamma distribution parameter and the LG model of amino acid substitution [38]. A non-parametric approximate likelihood ratio test based on a Shimodaira-Hasegawa-like procedure was used to calculate branch support values using PhyML 3.0 [38]. The trees were visualized in FigTree v1.4.4 and rooted with the respective *Saccharomyces cerevisiae* homologues (PAM16 or Yim1p).

CRISPR-Cas9 mutagenesis

CRISPR-Cas9 mutants were generated based on the protocols described in [77] and [78]. Guide RNAs (sgRNAs) annealing to different parts of the genes Mp*PAM16* (Mp3g09390.1) or Mp*RTN4IP1L* (Mp3g19030.1) were designed to be 5' of an "NGG" site (PAM sequence) as

required by the CRISPR-Cas9 system [77]. Guide RNAs were cloned into the pHB453 or pMpGE_En03 constructs [78] to generate the entry vectors using primers "sgRNA" (S3 Table). The expression vectors were generated by LR reaction of the destination vector pMpGE010 and the entry vectors. Vectors were transformed into *Escherichia coli* One Shot OmniMAX 2 T1R (Thermo Fisher Scientific: Cat. # C854003).

The expression vectors were transformed into *Agrobacterium tumefaciens* strain GV3101. Wild-type *M*. *polymorpha* spores from a cross between Tak-1 and Tak-2 accessions were transformed as per the protocol in [79]. Transformants were selected by growth on solid ½ Gamborg medium supplemented with 10 mg/l hygromycin B (Melford: CAS# 31282-04-9) to select for plants with the CRISPR-Cas9 construct insertion, and 100 mg/l cefotaxime (Melford: CAS# 64485-93-4) to kill any remaining *A*. *tumefaciens*.

To identify potential mutations in the Mp*PAM16* or Mp*RTN4IP1L* genes, genomic regions including the loci targeted by the guide RNAs were amplified by PCR and Sanger sequenced using primers "PAM16_G" or "RTN4IP1L_G" (S3 Table). Sanger sequencing of the purified PCR products was conducted by Source BioScience or by the Molecular Biology service at Vienna BioCenter Core Facilities (VBCF), member of the Vienna BioCenter (VBC), Austria. Mutants were named according to the gene mutated (Mp*pam16* or Mp*rtn4ip1l*), followed by "GE" (gene edited), the number of the guide RNA targeting the locus in which the mutation is found, and the number transformant that was genotyped (e.g. Mp*rtn4ip1l*^{GE149} –a gene edited transformant with a mutation in the *RTN4IP1L* gene at the locus targeted by sgRNA 1 which was the 49th transformant genotyped).

Generation of herbicide-resistant *M*. *polymorpha* lines via UV-B mutagenesis

Spores were mutagenized according to the protocol in [40]. Sterilised fresh wild type *M*. *polymorpha* spores were plated on solid modified Johnson's medium supplemented with thaxtomin A (5 μM–LD_{100}) or chlorsulfuron (140 nM– 4 x LD_{100}). The spores were exposed to UV-B irradiation (302 nm) for an exposure time corresponding to or near the LD_{50} (an exposure time of UV-B at which 50% of spores are killed–S2 Fig) using a UVP BioDoc-It. Plates of mutagenized spores were wrapped in aluminium foil and left in the dark overnight. Plates were then unwrapped and placed in a Sanyo growth chamber at 23˚C in 24-hour light. After 14 days of growth, plates were screened for surviving sporelings. Surviving sporelings were transferred to solid modified Johnson's medium supplemented with fresh herbicide. Plants which survived this second transfer onto a lethal dose of herbicide were maintained. To test for retention of resistance through asexual reproduction, gemmae from these plants were plated onto a lethal dose of herbicide. Lines whose resistance was inherited were classified as herbicide resistant lines and maintained. Lines with thaxtomin A resistance were named Mp*thar* (*th*axtomin *A* *r*esistant).

Chlorsulfuron-resistant lines were tested for target-site resistance by PCR amplification and Sanger sequencing of regions of the MpAHAS gene using primers GCS_Fw and GCS_Rv (S3 Table). Sanger sequencing of the purified PCR products was carried out by Source BioScience. Lines with target-site resistance to chlorsulfuron were named Mp*ahas*^{chlr} (Mp*ahas* *chl*orsulfuron *r*esistant).

Genomic DNA sequencing

Wild-type (Tak-1, Tak-2, OxTak1F, and OxTak2M) lines and herbicide-resistant lines (Mp*thar* and Mp*ahas*^{chlr}) were grown on solid ½ Gamborg medium for three weeks on in a growth chamber at 23˚C under 24-hour 10–30 μmol m^{-2} s^{-1} white light. After three weeks of

growth, plant material was harvested and flash frozen in liquid nitrogen. Samples were ground in liquid nitrogen and genomic DNA was extracted using the Qiagen DNeasy Plant Maxi kit (Cat. # 68163) according to the kit protocol. After elution, the gDNA was cleaned up and concentrated using the Zymo Genomic DNA Clean & Concentrator kit (Cat. # D4010). The gDNA was eluted in nuclease-free water.

The concentration of the gDNA was checked using a Nanodrop 1000 spectrophotometer and a Qubit 2.0 fluorometer according to the instruction manuals. The gDNA quality was checked by running 2 μl DNA (approximately 10 μg μl^{-1}) on a 0.7% agarose gel at 70 V for 45 minutes and checking for degradation. Genomic DNA samples which had passed quality control checks were sent for sequencing to the Next Generation Sequencing Facility at Vienna BioCenter Core Facilities (VBCF), member of the Vienna BioCenter (VBC), Austria. DNA Libraries were prepared using the Westburg NGS Library Prep kit and fragment size was determined using a BioLabTech Fragment Analyzer. The DNA was sequenced on an Illumina NovaSeq 6000 SP flowcell using 150 bp paired-end reads.

Non-allelism based SNP discovery pipeline

The "non-allelism based SNP discovery" pipeline from [40] was used with slight adaptations to identify candidate resistance-conferring SNPs in herbicide resistant lines. Raw reads were trimmed to remove low-quality reads and NEB adaptors using Trimmomatic 0.38 [80]. The read coverage was then normalized using khmer 2.1.2 [81]. Reads were aligned to the *Marchantia polymorpha* reference genome (MpTak1 v5.1 plus the female chromosome from v3.1; now known as MpTak v6.1) using bowtie2. Reads were sorted by position and reads from different lanes were merged using samtools 1.10. The variant call analysis was carried out using samtools and bcftools (ploidy defined as haploid, multiallelic/rare variant call option selected) to generate bcf files listing mismatches between the sequencing reads and the reference genome for each line [82]. For each bcf file, only mismatches which were supported by 7–100 reads and where the number of reads supporting high quality alternative alleles $\geq$ the number of reads supporting high quality reference alleles were retained (DP4[2]+DP4[3])/sum(DP4)$>$ 0.5). Non-canonical UV-B induced mismatches (not C ➔ T or G ➔ A) were filtered out using bcftools. Filtered mismatches were retained only if they were not present in other sequenced non-allelic lines without that phenotype. The resulting lists were filtered to retain only mismatches present in a CDS using bash scripting, then filtered manually in Interactive Genomics Viewer v 2.10 to remove mismatches which did not induce an amino acid change and which were misaligned or poor quality.

SNPs identified in the Mp*RTN4IP1L* gene in Mp*thar2*, Mp*thar4* and Mp*thar6* by the pipeline were confirmed by PCR amplification and Sanger sequencing using primers "GRT" (S3 Table). Sanger sequencing was carried out by Source BioScience.

Metabolomic analysis of pure and modified thaxtomin A in *M. polymorpha* thallus

Gemmae were grown on autoclaved cellophane (AA Packaging Limited, Preston, UK) on solid ½ Gamborg medium supplemented with 0.1% DMSO for 14 days at 23˚C in 24 h light (n = 6). Gemmalings were then transferred (by transfer of the cellophane disc) onto solid ½ Gamborg medium supplemented with either 0.1% DMSO or 5 μM thaxtomin A and grown in these conditions for 2 days at 23˚C in 24 h light. Treated and untreated gemmalings were harvested by flash freezing in liquid nitrogen.

For thaxtomin A analysis, frozen tissue samples were ground in liquid nitrogen and homogenized in ice-cold extraction solvent (2:1:1 methanol:acetonitrile:H_2O, v/v) for 2 min at 4˚C

followed by incubation at -20˚C for one hour. Samples were centrifuged at full speed at 4˚C for 3 mins. Supernatants were collected and kept at -20˚C. Pellets were redissolved in ice cold 80% (v/v) methanol and homogenized for 1 min at 4˚C followed by incubation at -20˚C for one hour. Samples were centrifuged at full speed at 4˚C for 3 mins. Supernatants were collected and added to the supernatants from the first extraction step. Samples were incubated at -20˚C for 2 hours. Samples were then centrifuged at full speed at 4˚C for 10 mins. Supernatants were collected and shock frozen in liquid nitrogen. For coenzyme Q10 analysis, a chloroform/methanol extraction from frozen plant tissue was carried out.

Metabolite extracts were analyzed by the Metabolomics Facility at Vienna BioCenter Core Facilities (VBCF), member of the Vienna BioCenter (VBC), Austria and funded by the Austrian Federal Ministry of Education, Science & Research and the City of Vienna. Thaxtomin A was analyzed by injecting 1 μl of each metabolite extract sample onto a Kinetex (Phenomenex) C18 column (100 Å, 150 x 2.1 mm) connected with the respective guard column, and employing a 4-minute-long linear gradient from 96% A (1% acetonitrile, 0.1% formic acid in water) to 90% B (0.1% formic acid in acetonitrile) at a flow rate of 80 μl/min. Detection and quantification was done by LC-MS/MS, employing the selected reaction monitoring (SRM) mode of a TSQ Altis mass spectrometer (Thermo Fisher Scientific), using the following transitions in the positive ion mode: 439.1 *m/z* to 247.1 *m/z* and 439.1 *m/z* to 219.1 *m/z*. Quantification was done by external calibration using an authentic standard. The putative thaxtomin A metabolite (without the nitro-functionality) was discovered by analyzing the samples with precursor ion scanning for the dominant fragment ion (*m/z* 247.1) of thaxtomin A. Here only one compound was evident with a *m/z* of 394, sharing both dominant fragment ions (*m/z* 247.1 and *m/z* 219.1) with thaxtomin A). This metabolite was analyzed in the samples using the transitions 394.1 *m/z* to 247.1 *m/z* and 394.1 *m/z* to 219.1 *m/z*. Data interpretation was performed using TraceFinder (Thermo Fisher Scientific).

Coenzyme Q10 was analyzed after chloroform/methanol extraction from powdered frozen plant tissue. 100 μl of the lower phase was diluted with 50 μl methanol and 1 μl was directly injected onto a Kinetex (Phenomenex) C8 column (100 Å, 100 x 2.1 mm) and employing a 5-minute-long linear gradient from 90% A (50% acetonitrile, 49.9% water, 0.1% formic acid, 10 mM ammonium formate) to 95% B (10% acetonitrile 88% isopropanol, 1.9% water, 0.1% formic acid, 10 mM ammonium formate) at a flow rate of 100 μl/min. Detection and quantification was done by LC-MS/MS, employing the selected reaction monitoring (SRM) mode of a TSQ Altis mass spectrometer (Thermo Fisher Scientific), using the transition 863.8 *m/z* to 197.1 *m/z* in the positive ion mode.

DAB staining

3,3'-diaminobenzidine (DAB) (Sigma Aldrich: D8001) was used to prepare a DAB staining solution according to [50]. Tak-1, Tak-2, Mp*rtn4ip1l*^{GE118} and Mp*rtn4ip1l*^{GE149} 11-day old plants were incubated in 3 ml solution in 24 well plates and vacuum infiltrated for 5 minutes (n = 3). The plates were covered in aluminium foil and incubated for 1.5 hours shaking at 100 rpm. After incubation, the staining solution was replaced by bleaching solution prepared according to [50]. Plants were bleached for 2 hours. Bleached gemmae were imaged using a Keyence VHX-7000.

Ferric-xylenol orange (FOX) assay

A modified FOX assay was carried out according to the protocol in [52]. The FOX working solution was prepared as follows: 500 μM ammonium ferrous sulphate; 400 μM xylenol orange; 200 mM sorbitol; 25 mM H_2SO_4. Twelve-day old gemmalings of Tak-1, Tak-2,

Table 2. Components of ½ Gamborg medium.

Component	Source	Final concentration
Gamborg B5 medium basal salt mixture	Sigma Aldrich (G5768)	1.5 g/l (w/v)
MES monohydrate	Applichem (A1074)	0.5 g/l (w/v)
Sucrose	Applichem (A2211)	1% (w/v)
Agar	Applichem (A2111)	0.8% (w/v)

Components used to make up ½ Gamborg medium. The pH was adjusted to 5.5 using 1 M KOH.

https://doi.org/10.1371/journal.pgen.1010423.t002

Mp*rtn4ip1l*^{GE118} and Mp*rtn4ip1l*^{GE149} were frozen and ground in liquid nitrogen and homogenized in 200 mM perchloric acid (n = 3). Samples were centrifuged at 1000g for 5 minutes at 4˚C. 500 μl of the supernatant were mixed with 500 μl FOX working solution. Samples were incubated at room temperature in the dark for 30 minutes followed by quantification of the absorbance at 560 nm using an Ultrospec 3100 pro spectrophotometer. The concentration of H_2O_2 in each sample was calculated using a calibration curve of known concentrations of H_2O_2 quantified using the same protocol.

Media

Modified Johnson's medium was prepared as described in [79].

½ Gamborg medium was prepared using the following components (Table 2):

Supporting information

S1 Fig. Amino acid alignments of PAM16 homologues and mutations identified in Mp*pam16* mutants. (A) Trimmed amino acid alignment of PAM16 homologues. Protein sequences similar to AtPAM16 (At3G59280) from 11 species were identified using the BlastP algorithm to search their proteomes [37]. The sequences were aligned via the L-INS-i strategy in MAFFT [76] and manually trimmed. The predicted signal peptides are marked in red and magnified in **(B)**. **(C)** Mp*pam16* mutants were generated via CRISPR-Cas9 mutagenesis to target the Mp*PAM16* gene. Wild type spores (Tak-1 x Tak-2) were transformed with *Agrobacterium tumefaciens* strains carrying the vector containing the Cas9 gene and an sgRNA targeting Mp*PAM16*. Positive transformants were genotyped using Sanger sequencing to determine the mutations induced by the CRISPR-Cas9 complex. Predicted protein sequences were determined based on the mutations in each line. Nucleotide or protein sequences were aligned via the L-INS-i strategy using MAFFT version 7. The top row is the reference Mp*PAM16* nucleotide sequence or the reference MpPAM16 protein sequence (MpTak v6.1).
(TIF)

S2 Fig. Dose-response curve of UV-B radiation on *M. polymorpha* spores. Wild type spores (from a cross between Tak-1 and Tak-2) were plated on solid medium and subjected to UV-B irradiation for different lengths of time using a UVP BioDoc-It. Spores were imaged after 14 days of growth using a Leica DFC310 FX stereomicroscope. The total area of spores on each plate was determined using ImageJ (Tab D in S1 Table). The fitted curve was calculated using the four-parameter log-logistic equation from the drc package in R. IC_{50} (exposure time of UV-B at which the average sporeling area on the plate was reduced by 50%) was calculated from the dose-response curve as approximately 110 s. Error bars represent ± standard deviation (n = 3).
(TIF)

S3 Fig. Sanger sequencing of the Mp3g19030.1 gene in Mp*thar* mutants and amino acid alignment of RTN4IP1 homologues. (A, B, and C) Regions of the Mp3g19030.1 gene in Mp*thar2* **(A)**, Mp*thar4* **(B)**, and Mp*thar6* **(C)** were Sanger sequenced to confirm the SNPs identified by next generation sequencing. The consensus sequence is shown on the top rows, and results from the Sanger sequencing are shown on the second rows. The blue arrows indicate the site of mutation in each Mp*thar* mutant, and the tick marks above the sequences indicate the position of the nucleotide in the Mp3g19030.1 gene. **(D)** Trimmed amino acid alignment of RTN4IP1 homologues. Protein sequences similar to HsRTN4IP1 from 10 species were identified using the BlastP algorithm to search their proteomes [37]. The sequences were aligned via the L-INS-i strategy in MAFFT [76] and manually trimmed.
(TIF)

S4 Fig. Nucleotide and amino acid alignments of the Mp*RTN4IP1L* genes and MpRTN4IP1L proteins of Mp*rtn4ip1l* mutants. Mp*rtn4ip1l* mutants were generated via CRISPR-Cas9 mutagenesis to target the Mp*RTN4IP1L* gene. Wild type spores (Tak-1 x Tak-2) were transformed with *Agrobacterium tumefaciens* strains carrying the vectors containing the Cas9 gene and an sgRNA targeting Mp*RTN4IP1L*: **(A)** sgRNA1, **(B)** sgRNA 2, **(C)** sgRNA3. Positive transformants were genotyped using Sanger sequencing to determine the mutations induced by the CRISPR-Cas9 complex. Predicted protein sequences were determined based on the mutations in each line. Nucleotide or protein sequences were aligned via the L-INS-i strategy using MAFFT version 7 [76]. The top row is the reference Mp*RTN4IP1L* nucleotide sequence or the reference MpRTN4IP1L protein sequence (MpTak v6.1).
(TIF)

S5 Fig. Sanger sequencing of Mp$ahas^{chlr}$ mutants. Regions of the Mp*AHAS* gene (Mp7g01940.1) in each Mp$ahas^{chlr}$ mutant were Sanger sequenced to identify any target-site resistance conferring mutations. The consensus sequence is shown on the top rows, and results from the Sanger sequencing are shown on the subsequent rows. The blue arrows indicate the site of mutation in each Mp$ahas^{chlr}$ mutant, and the tick marks above the sequences indicate the position of the nucleotide in the Mp*AHAS* gene.
(TIF)

S6 Fig. LC-MS/MS analysis of thaxtomin A and its putative metabolite in wild type and Mp*rtn4ip1l* mutant extracts. Gemmalings from each line were grown on solid medium supplemented with 0.1% DMSO for 14 days, then transferred to solid ½ Gamborg medium supplemented with 5 μM thaxtomin A or 0.1% DMSO and grown for 2 days. Cellular fractions were extracted from thaxtomin A-treated and untreated samples. **(A)** A precursor ion analysis of samples from Tak-2 and Mp$rtn4ip1l^{GE118}$ mutants was conducted via LC-MS/MS (n = 6). Chromatograms of the total ion currents of precursor ion scanning for *m/z* 247.1 are depicted. The peak eluting at a retention time of 8.99 min is Thaxtomin A (*m/z* 439.1), the peak eluting at a retention time of 9.25 min (*m/z* 394.1) is its putative metabolite. Both peaks are absent in the analysis of the untreated samples. **(B)** MS/MS of *m/z* 439.2 from thaxtomin A treated samples. The fragment ions *m/z* 219.1 and *m/z* 247.1 are identical to the fragment ions observed in the authentic standard of thaxtomin A and reported in the literature [83]. **(C)** MS/MS spectra of the unknown compound eluting at a RT of 9.25 min. Both prominent fragment ions of thaxtomin A are present. **(D)** A precursor ion analysis of samples from Tak-1 and Mp$rtn4ip1l^{GE149}$ mutants was conducted via LC-MS/MS (n = 6). Chromatograms of the total ion currents of precursor ion scanning for *m/z* 247.1 are depicted. The peak eluting at a retention time of 8.99 min is Thaxtomin A (*m/z* 439.1), the peak eluting at a retention time of 9.25 min (*m/z* 394.1) is its putative metabolite.
(TIF)

S1 Table. Numerical data underlying graphs and summary statistics.
(XLSX)

S2 Table. Homologues of the *A. thaliana* gene AT3G59280 identified by BlastP search (E value < 1E-5).
(XLSX)

S3 Table. Primer list.
(XLSX)

S1 Text. Amino acid sequences and tree files used to build phylogenetic trees for PAM16 and RTN4IP1 homologues.
(RTF)

Acknowledgments

We thank Laura Moody and Franck Dayan for suggestions. We thank Alex Casey and Sam Caygill for discussions about herbicide resistance and comments on the manuscript. We thank Sandy Hetherington for help with phylogenetic analyses. We thank the Next Generation Sequencing Facility at the Vienna BioCenter Core Facilities (VBCF) for library preparation and sequencing of genomic DNA samples.

Author Contributions

Conceptualization: Chloe Casey, Liam Dolan.

Data curation: Chloe Casey, Thomas Köcher, Clément Champion.

Formal analysis: Chloe Casey.

Funding acquisition: Liam Dolan.

Investigation: Chloe Casey, Thomas Köcher, Katharina Jandrasits, Magdalena Mosiolek.

Methodology: Chloe Casey, Clément Champion, Katharina Jandrasits, Magdalena Mosiolek.

Project administration: Liam Dolan.

Resources: Clémence Bonnot.

Software: Clément Champion.

Supervision: Liam Dolan.

Visualization: Chloe Casey.

Writing – original draft: Chloe Casey.

Writing – review & editing: Chloe Casey, Thomas Köcher, Liam Dolan.

References

1. Gaines TA, Duke SO, Morran S, Rigon CAG, Tranel PJ, Kupper A, et al. Mechanisms of evolved herbicide resistance. Journal of Biological Chemistry. 2020; 295(30):10307–30. https://doi.org/10.1074/jbc.REV120.013572 PMID: 32430396
2. Heap I. The International Survey of Herbicide Resistant Weeds 2022 [Available from: http://www.weedscience.org/Home.aspx.
3. Powles S, Yu Q, Merchant S, Briggs W, Ort D. Evolution in Action: Plants Resistant to Herbicides. Annual Review of Plant Biology, Vol 61. 2010;61:317–47. https://doi.org/10.1146/annurev-arplant-042809-112119 PMID: 20192743

4. Delye C, Jasieniuk M, Le Corre V. Deciphering the evolution of herbicide resistance in weeds. Trends in Genetics. 2013; 29(11):649–58. https://doi.org/10.1016/j.tig.2013.06.001 PMID: 23830583

5. Rojano-Delgado AM, Portugal JM, Palma-Bautista C, Alcantara-de la Cruz R, Torra J, Alcantara E, et al. Target site as the main mechanism of resistance to imazamox in a Euphorbia heterophylla biotype. Scientific Reports. 2019;9.

6. Yuan JS, Tranel PJ, Stewart CN. Non-target-site herbicide resistance: a family business. Trends in Plant Science. 2007; 12(1):6–13. https://doi.org/10.1016/j.tplants.2006.11.001 PMID: 17161644

7. Cummins I, Cole DJ, Edwards R. A role for glutathione transferases functioning as glutathione peroxidases in resistance to multiple herbicides in black-grass. Plant Journal. 1999; 18(3):285–92. https://doi.org/10.1046/j.1365-313x.1999.00452.x PMID: 10377994

8. Cummins I, Bryant DN, Edwards R. Safener responsiveness and multiple herbicide resistance in the weed black-grass (Alopecurus myosuroides). Plant Biotechnology Journal. 2009; 7(8):807–20. https://doi.org/10.1111/j.1467-7652.2009.00445.x PMID: 19754839

9. Cummins I, Wortley DJ, Sabbadin F, He Z, Coxon CR, Straker HE, et al. Key role for a glutathione transferase in multiple-herbicide resistance in grass weeds. Proceedings of the National Academy of Sciences of the United States of America. 2013; 110(15):5812–7. https://doi.org/10.1073/pnas.1221179110 PMID: 23530204

10. Gressel J. Molecular biology of weed control. Transgenic Research. 2000; 9(4–5):355–82. https://doi.org/10.1023/a:1008946628406 PMID: 11131013

11. Amrhein N, Deus B, Gehrke P, Steinrucken HC. The Site of the Inhibition of the Shikimate Pathway by Glyphosate: II. Interference of Glyphosate with Chorismate Formation In Vivo and In Vitro. Plant Physiol. 1980; 66(5):830–4. https://doi.org/10.1104/pp.66.5.830 PMID: 16661535

12. Zhang C, Yu CJ, Yu Q, Guo WL, Zhang TJ, Tian XS. Evolution of multiple target-site resistance mechanisms in individual plants of glyphosate-resistant Eleusine indica from China. Pest Management Science. 2021; 77(10):4810–7. https://doi.org/10.1002/ps.6527 PMID: 34161662

13. Gaines TA, Zhang WL, Wang DF, Bukun B, Chisholm ST, Shaner DL, et al. Gene amplification confers glyphosate resistance in Amaranthus palmeri. Proceedings of the National Academy of Sciences of the United States of America. 2010; 107(3):1029–34. https://doi.org/10.1073/pnas.0906649107 PMID: 20018685

14. Han HP, Yu Q, Beffa R, Gonzalez S, Maiwald F, Wang J, et al. Cytochrome P450 CYP81A10v7 in Lolium rigidum confers metabolic resistance to herbicides across at least five modes of action. Plant Journal. 2021; 105(1):79–92. https://doi.org/10.1111/tpj.15040 PMID: 33098711

15. Pan L, Yu Q, Wang JZ, Han HP, Mao LF, Nyporko A, et al. An ABCC-type transporter endowing glyphosate resistance in plants. Proceedings of the National Academy of Sciences of the United States of America. 2021; 118(16). https://doi.org/10.1073/pnas.2100136118 PMID: 33846264

16. Vila-Aiub M, Yu Q, Powles S. Do plants pay a fitness cost to be resistant to glyphosate? New Phytologist. 2019;223.

17. Kreiner JM, Giacomini DA, Bemm F, Waithaka B, Regalado J, Lanz C, et al. Multiple modes of convergent adaptation in the spread of glyphosate-resistant Amaranthus tuberculatus. Proceedings of the National Academy of Sciences of the United States of America. 2019; 116(42):21076–84. https://doi.org/10.1073/pnas.1900870116 PMID: 31570613

18. Van Etten M, Lee KM, Chang SM, Baucom RS. Parallel and nonparallel genomic responses contribute to herbicide resistance in Ipomoea purpurea, a common agricultural weed. Plos Genetics. 2020; 16(2). https://doi.org/10.1371/journal.pgen.1008593 PMID: 32012153

19. Kreiner JM, Tranel PJ, Weigel D, Stinchcombe JR, Wright SI. The genetic architecture and population genomic signatures of glyphosate resistance in Amaranthus tuberculatus. Molecular Ecology. 2021; 30(21):5373–89. https://doi.org/10.1111/mec.15920 PMID: 33853196

20. Scheible W, Fry B, Kochevenko A, Schindelasch D, Zimmerli L, Somerville S, et al. An Arabidopsis mutant resistant to thaxtomin A, a cellulose synthesis inhibitor from Streptomyces species. Plant Cell. 2003; 15(8):1781–94. https://doi.org/10.1105/tpc.013342 PMID: 12897252

21. Reavell-Roy E. Forward screening for herbicide resistance in Arabidopsis thaliana and the monocot species Triticum aestivum. University of Ontario Institute of Technology: University of Ontario Institute of Technology; 2019.

22. King R, Lawrence C, Clark M, Calhoun L. ISOLATION AND CHARACTERIZATION OF PHYTOTOXINS ASSOCIATED WITH STREPTOMYCES SCABIES. Journal of the Chemical Society-Chemical Communications. 1989(13):849–50.

23. King R, Lawrence C, Gray J. Herbicidal Properties of the thaxtomin Group of phytotoxins. Journal of Agricultural and Food Chemistry. 2001; 49(5):2298–301. https://doi.org/10.1021/jf0012998 PMID: 11368592

24. King R, Calhoun L. The thaxtomin phytotoxins: Sources, synthesis, biosynthesis, biotransformation and biological activity. Phytochemistry. 2009; 70(7):833–41. https://doi.org/10.1016/j.phytochem.2009.04.013 PMID: 19467551

25. Shrestha U, Duesterbeck G, Rosskopf E, Butler D. Evaluation of a Bioherbicide and Anaerobic Soil Disinfestation for Weed Control in Specialty Crop Production. Annual International Research Conference on Methyl Bromide Alternatives and Emissions Reductions; Maitland, Florida2016.

26. Marrone Bio Innovations I. Marrone Bio Advances Novel Herbicides Davis, California, 2021 [Available from: https://marronebio.com/marrone-bio-advances-novel-herbicides/.

27. Leep DC, Doricchi L, Perez Baz MJ, Millan FR, Fernandez Chimeno RI, inventorsUse of thaxtomin for selective control of rice and aquatic based weeds. United States2010.

28. Koivunen M, Marrone P, inventors; Marrone Bio Innovations, Inc., assignee. Uses of thaxtomin and thaxtomin compositions as herbicides. US2010.

29. Fry BA, Loria R. Thaxtomin A: evidence for a plant cell wall target. Physiological and Molecular Plant Pathology. 2002; 60(1):1–8.

30. Tateno M, Brabham C, DeBolt S. Cellulose biosynthesis inhibitors—a multifunctional toolbox. Journal of Experimental Botany. 2016; 67(2):533–42. https://doi.org/10.1093/jxb/erv489 PMID: 26590309

31. Frazier AE, Dudek J, Guiard B, Voos W, Li YF, Lind M, et al. Pam16 has an essential role in the mitochondrial protein import motor. Nature Structural & Molecular Biology. 2004; 11(3):226–33. https://doi.org/10.1038/nsmb735 PMID: 14981507

32. Huang Y, Chen XJ, Liu YA, Roth C, Copeland C, McFarlane HE, et al. Mitochondrial AtPAM16 is required for plant survival and the negative regulation of plant immunity. Nature Communications. 2013; 4:13. https://doi.org/10.1038/ncomms3558 PMID: 24153405

33. Ishizaki K, Nishihama R, Yamato K, Kohchi T. Molecular Genetic Tools and Techniques for Marchantia polymorpha Research. Plant and Cell Physiology. 2016; 57(2):262–70. https://doi.org/10.1093/pcp/pcv097 PMID: 26116421

34. Kohchi T, Yamato KT, Ishizaki K, Yamaoka S, Nishihama R. Development and Molecular Genetics of Marchantia polymorpha. Annual Review of Plant Biology, Vol 72, 2021. 2021; 72:677–702. https://doi.org/10.1146/annurev-arplant-082520-094256 PMID: 33684298

35. Ligrone R, Duckett JG, Renzaglia KS. Major transitions in the evolution of early land plants: a bryological perspective. Ann Bot. 1092012. p. 851–71. https://doi.org/10.1093/aob/mcs017 PMID: 22356739

36. Pires ND, Dolan L. Morphological evolution in land plants: new designs with old genes. Philos Trans R Soc Lond B Biol Sci. 3672012. p. 508–18. https://doi.org/10.1098/rstb.2011.0252 PMID: 22232763

37. Altschul SF, Gish W, Miller W, Myers EW, Lipman DJ. Basic Local Alignment Search Tool. Journal of Molecular Biology. 1990; 215(3):403–10. https://doi.org/10.1016/S0022-2836(05)80360-2 PMID: 2231712

38. Guindon S, Dufayard JF, Lefort V, Anisimova M, Hordijk W, Gascuel O. New Algorithms and Methods to Estimate Maximum-Likelihood Phylogenies: Assessing the Performance of PhyML 3.0. Systematic Biology. 2010; 59(3):307–21. https://doi.org/10.1093/sysbio/syq010 PMID: 20525638

39. Gardner SN, Gressel J, Mangel M. A revolving dose strategy to delay the evolution of both quantitative vs major monogene resistances to pesticides and drugs. International Journal of Pest Management. 1998; 44(3):161–80.

40. Champion C, Lamers J, Jones VAS, Morieri G, Honkanen S, Dolan L. Microtubule associated protein WAVE DAMPENED2-LIKE (WDL) controls microtubule bundling and the stability of the site of tip-growth in Marchantia polymorpha rhizoids. Plos Genetics. 2021; 17(6):20. https://doi.org/10.1371/journal.pgen.1009533 PMID: 34086675

41. Hartman PS, Herman RK. RADIATION-SENSITIVE MUTANTS OF CAENORHABDITIS-ELEGANS. Genetics. 1982; 102(2):159–78. https://doi.org/10.1093/genetics/102.2.159 PMID: 7152245

42. Park I, Kim K-e, Kim J, Bae S, Jung M, Choi J, et al. In vivo mitochondrial matrix proteome profiling reveals RTN4IP1/OPA10 as an antioxidant NADPH oxidoreductase. bioRxiv. 2021:2021.10.14.464368.

43. Trentmann O, Muhlhaus T, Zimmer D, Sommer F, Schroda M, Haferkamp I, et al. Identification of Chloroplast Envelope Proteins with Critical Importance for Cold Acclimation(1) (OPEN). Plant Physiology. 2020; 182(3):1239–55.

44. Miras S, Salvi D, Ferro M, Grunwald D, Garin J, Joyard J, et al. Non-canonical transit peptide for import into the chloroplast. Journal of Biological Chemistry. 2002; 277(49):47770–8. https://doi.org/10.1074/jbc.M207477200 PMID: 12368288

45. Senkler J, Senkler M, Eubel H, Hildebrandt T, Lengwenus C, Schertl P, et al. The mitochondrial complexome of Arabidopsis thaliana. Plant Journal. 2017; 89(6):1079–92. https://doi.org/10.1111/tpj.13448 PMID: 27943495

46. Zhao RZ, Jiang S, Zhang L, Yu ZB. Mitochondrial electron transport chain, ROS generation and uncoupling (Review). International Journal of Molecular Medicine. 2019; 44(1):3–15. https://doi.org/10.3892/ijmm.2019.4188 PMID: 31115493

47. Bentinger M, Brismar K, Dallner G. The antioxidant role of coenzyme Q. Mitochondrion. 2007; 7:S41–S50. https://doi.org/10.1016/j.mito.2007.02.006 PMID: 17482888

48. Genova ML, Lenaz G. New developments on the functions of coenzyme Q in mitochondria. Biofactors. 2011; 37(5):330–54. https://doi.org/10.1002/biof.168 PMID: 21989973

49. Bersuker K, Hendricks JM, Li ZP, Magtanong L, Ford B, Tang PH, et al. The CoQ oxidoreductase FSP1 acts parallel to GPX4 to inhibit ferroptosis. Nature. 2019; 575(7784):688–92. https://doi.org/10.1038/s41586-019-1705-2 PMID: 31634900

50. Daudi A, O'Brien JA. Detection of Hydrogen Peroxide by DAB Staining in Arabidopsis Leaves. Bio-protocol. 2012; 2(18):e263. PMID: 27390754

51. Gay C, Collins J, Gebicki JM. Hydroperoxide assay with the ferric-xylenol orange complex. Analytical Biochemistry. 1999; 273(2):149–55. https://doi.org/10.1006/abio.1999.4208 PMID: 10469484

52. Li Z-G. Chapter 5—Measurement of Signaling Molecules Calcium Ion, Reactive Sulfur Species, Reactive Carbonyl Species, Reactive Nitrogen Species, and Reactive Oxygen Species in Plants. In: Khan MIR, Reddy PS, Ferrante A, Khan NA, editors. Plant Signaling Molecules: Woodhead Publishing; 2019. p. 83–103.

53. Fukushima T, Yamada K, Isobe A, Shiwaku K, Yamane Y. Mechanism of cytotoxicity of paraquat. 1. NADH oxidation and paraquat radical formation via Complex I. Experimental and Toxicologic Pathology. 1993; 45(5–6):345–9.

54. Hawkes TR. Mechanisms of resistance to paraquat in plants. Pest Management Science. 2014; 70 (9):1316–23. https://doi.org/10.1002/ps.3699 PMID: 24307186

55. Takano HK, Beffa R, Preston C, Westra P, Dayan FE. Reactive oxygen species trigger the fast action of glufosinate. Planta. 2019; 249(6):1837–49. https://doi.org/10.1007/s00425-019-03124-3 PMID: 30850862

56. Duke SO, Lydon J, José MB, Sherman TD, Lehnen LP, Matsumoto H. Protoporphyrinogen Oxidase-Inhibiting Herbicides. Weed Science. 1991; 39(3):465–73.

57. Awwad F, Bertrand G, Grandbois M, Beaudoin N. Reactive Oxygen Species Alleviate Cell Death Induced by Thaxtomin A in Arabidopsis thaliana Cell Cultures. Plants-Basel. 2019; 8(9):332. https://doi.org/10.3390/plants8090332 PMID: 31489878

58. Kaloumenos NS, Tsioni VC, Daliani EG, Papavassileiou SE, Vassileiou AG, Laoutidou PN, et al. Multiple Pro-197 substitutions in the acetolactate synthase of rigid ryegrass (Lolium rigidum) and their impact on chlorsulfuron activity and plant growth. Crop Protection. 2012; 38:35–43.

59. Zhang Y, Xu Y, Wang S, Li X, Zheng M. Resistance mutations of Pro197, Asp376 and Trp574 in the acetohydroxyacid synthase (AHAS) affect pigments, growths, and competitiveness of Descurainia sophia L. Scientific Reports. 2017; 7(1):16380. https://doi.org/10.1038/s41598-017-16655-0 PMID: 29180697

60. Shim I, Law R, Kileeg Z, Stronghill P, Northey JGB, Strap JL, et al. Alleles Causing Resistance to Isoxaben and Flupoxam Highlight the Significance of Transmembrane Domains for CESA Protein Function. Frontiers in Plant Science. 2018; 9:14.

61. Acebes J, Encina A, García-Angulo P, Alonso-Simon A, Mélida H, Fernandez JA. Cellulose Biosynthesis Inhibitors: their uses as potential herbicides and as tools in cellulose and cell wall structural plasticity research. In: Lejeune A, Deprez T, editors. Cellulose: Structure and Properties, Derivatives and Industrial Uses 2010. p. 39–73.

62. Song YL. Insight into the mode of action of 2,4-dichlorophenoxyacetic acid (2,4-D) as an herbicide. Journal of Integrative Plant Biology. 2014; 56(2):106–13. https://doi.org/10.1111/jipb.12131 PMID: 24237670

63. Jeschke P. Propesticides and their use as agrochemicals. Pest Management Science. 2016; 72 (2):210–25. https://doi.org/10.1002/ps.4170 PMID: 26449612

64. Denness L, McKenna JF, Segonzac C, Wormit A, Madhou P, Bennett M, et al. Cell Wall Damage-Induced Lignin Biosynthesis Is Regulated by a Reactive Oxygen Species- and Jasmonic Acid-Dependent Process in Arabidopsis. Plant Physiology. 2011; 156(3):1364–74. https://doi.org/10.1104/pp.111.175737 PMID: 21546454

65. Brisson LF, Tenhaken R, Lamb C. FUNCTION OF OXIDATIVE CROSS-LINKING OF CELL-WALL STRUCTURAL PROTEINS IN PLANT-DISEASE RESISTANCE. Plant Cell. 1994; 6(12):1703–12. https://doi.org/10.1105/tpc.6.12.1703 PMID: 12244231

66. Tenhaken R. Cell wall remodeling under abiotic stress. Frontiers in Plant Science. 2015;5.

67. Bradley DJ, Kjellbom P, Lamb CJ. Elicitor-Induced and Wound-Induced Oxidative Cross-Linking of a Proline-Rich Plant-Cell Wall Protein—A Novel, Rapid Defense Response. Cell. 1992; 70(1):21–30.

68. Awwad F, Bertrand G, Grandbois M, Beaudoin N. Auxin protects Arabidopsis thaliana cell suspension cultures from programmed cell death induced by the cellulose biosynthesis inhibitors thaxtomin A and isoxaben. Bmc Plant Biology. 2019; 19(1):13.

69. Vila-Aiub MM, Neve P, Powles SB. Resistance cost of a cytochrome P450 herbicide metabolism mechanism but not an ACCase target site mutation in a multiple resistant Lolium rigidum population. New Phytol. 2005; 167(3):787–96. https://doi.org/10.1111/j.1469-8137.2005.01465.x PMID: 16101915

70. Tardif FJ, Rajcan I, Costea M. A mutation in the herbicide target site acetohydroxyacid synthase produces morphological and structural alterations and reduces fitness in Amaranthus powellii. New Phytologist. 2006; 169(2):251–64. https://doi.org/10.1111/j.1469-8137.2005.01596.x PMID: 16411929

71. Menchari Y, Chauvel B, Darmency H, Delye C. Fitness costs associated with three mutant acetyl-coenzyme A carboxylase alleles endowing herbicide resistance in black-grass Alopecurus myosuroides. Journal of Applied Ecology. 2008; 45(3):939–47.

72. Vila-Aiub MM, Neve P, Powles SB. Evidence for an ecological cost of enhanced herbicide metabolism in Lolium rigidum. Journal of Ecology. 2009; 97(4):772–80.

73. Ishizaki K, Chiyoda S, Yamato KT, Kohchi T. Agrobacterium-mediated transformation of the haploid liverwort Marchantia polymorpha L., an emerging model for plant biology. Plant and Cell Physiology. 2008; 49(7):1084–91. https://doi.org/10.1093/pcp/pcn085 PMID: 18535011

74. Wickham H. ggplot2 Elegant Graphics for Data Analysis Introduction. Ggplot2: Elegant Graphics for Data Analysis. Use R. New York: Springer; 2009. p. 1-+.

75. Ritz C, Baty F, Streibig JC, Gerhard D. Dose-Response Analysis Using R. Plos One. 2015; 10(12):13. https://doi.org/10.1371/journal.pone.0146021 PMID: 26717316

76. Katoh K, Rozewicki J, Yamada KD. MAFFT online service: multiple sequence alignment, interactive sequence choice and visualization. Briefings in Bioinformatics. 2019; 20(4):1160–6. https://doi.org/10.1093/bib/bbx108 PMID: 28968734

77. Sugano SS, Shirakawa M, Takagi J, Matsuda Y, Shimada T, Hara-Nishimura I, et al. CRISPR/Cas9-Mediated Targeted Mutagenesis in the Liverwort Marchantia polymorpha L. Plant and Cell Physiology. 2014; 55(3):475–81. https://doi.org/10.1093/pcp/pcu014 PMID: 24443494

78. Thamm A, Saunders TE, Dolan L. MpFEW RHIZOIDS1 miRNA-Mediated Lateral Inhibition Controls Rhizoid Cell Patterning in Marchantia polymorpha. Current Biology. 2020; 30(10):1905–15. https://doi.org/10.1016/j.cub.2020.03.032 PMID: 32243863

79. Honkanen S, Jones VAS, Morieri G, Champion C, Hetherington AJ, Kelly S, et al. The Mechanism Forming the Cell Surface of Tip-Growing Rooting Cells Is Conserved among Land Plants. Current Biology. 2016; 26(23):3238–44. https://doi.org/10.1016/j.cub.2016.09.062 PMID: 27866889

80. Bolger AM, Lohse M, Usadel B. Trimmomatic: a flexible trimmer for Illumina sequence data. Bioinformatics. 2014; 30(15):2114–20. https://doi.org/10.1093/bioinformatics/btu170 PMID: 24695404

81. Crusoe MR, Alameldin HF, Awad S, Boucher E, Caldwell A, Cartwright R, et al. The khmer software package: enabling efficient nucleotide sequence analysis. F1000Res. 2015; 4:900. https://doi.org/10.12688/f1000research.6924.1 PMID: 26535114

82. Danecek P, Bonfield JK, Liddle J, Marshall J, Ohan V, Pollard MO, et al. Twelve years of SAMtools and BCFtools. Gigascience. 2021; 10(2):4. https://doi.org/10.1093/gigascience/giab008 PMID: 33590861

83. Winn M, Francis D, Micklefield J. De novo Biosynthesis of "Non-Natural" Thaxtomin Phytotoxins. Angewandte Chemie-International Edition. 2018; 57(23):6830–3. https://doi.org/10.1002/anie.201801525 PMID: 29603527